Electronic Supplementary Material (ESI) for Inorganic Chemistry Frontiers.

Electronic Supplementary Information

Impacts of Coordination Modes on Red-Emitting Cyclometalated Iridium Complexes

Chenggang Jiang and Thomas S. Teets*

University of Houston, Department of Chemistry 3585 Cullen Blvd., Room 112, Houston, TX USA 77204-5003.

*Corresponding author: tteets@uh.edu

Experimental section

Materials

Solvents for photophysical and electrochemical measurements were obtained from a Grubbs Solvent Purification System and degassed with argon. Commercially available starting materials and reagents were used without further purification. Tetrabutylammonium hexafluorophosphate, used as a supporting electrolyte for cyclic voltammetry experiments, was recrystallized from hot ethanol, and ferrocene, used as an internal standard for cyclic voltammetry experiments, was purified by sublimation. The iridium dimers of the general formula $[Ir(C^N)_2(\mu\text{-}Cl)]_2$ (C^N = cyclometalating ligand) were prepared by following literature procedures,[1] refluxing $IrCl_3 \cdot xH_2O$ with 2.1 equivalents of the C^N ligand in a 3 : 1 2-methoxyethanol/water mixture. All the ancillary ligands used in this study were prepared following literature procedures.[2–5]

Physical Methods

^1H, and $^{13}C\{^1H\}$ NMR spectra were recorded at room temperature using a JEOL ECA-400, ECA-500, or ECA-600 NMR spectrometer. The ESI-MS experiments were conducted at The University of Texas at Austin's Mass Spectrometry Facility or Texas A&M University Chemistry Department Mass Spectrometry Facility. UV−vis absorption spectra were measured in toluene solutions in 1 cm quartz cuvettes sealed with a screw cap and septum, using an Agilent Cary 8454 UV−vis spectrophotometer. Steady-state emission spectra were measured using a Horiba FluoroMax-4 spectrofluorometer with appropriate long-pass filters to exclude stray excitation light from detection. To exclude air, samples for emission spectra were prepared in a nitrogen-filled glovebox using dry, deoxygenated solvents, and thin-film PMMA samples were kept under nitrogen until immediately before measurement. Emission quantum yields were determined relative to a standard of tetraphenylporphyrin (TPP) in toluene, which has a reported fluorescence quantum yield (Φ_F) of 0.11.[6] The absolute quantum yields of complexes doped into poly(methyl methacrylate) (PMMA) thin films were recorded using a Spectralon-coated integrating sphere integrated with a Horiba FluoroMax-4 spectrofluorometer. Cyclic voltammetry (CV) measurements were performed with a CH Instruments 602E potentiostat using a three-electrode system in a nitrogen-filled glovebox. A 3 mm diameter glassy-carbon electrode, Pt wire, and silver wire were used as the working electrode, counter electrode, and pseudoreference electrode, respectively. Measurements were performed in acetonitrile solution with 0.1 M $TBAPF_6$ as a supporting electrolyte at a scan rate of 0.1 V/s. Ferrocene was used as an internal standard, and potentials were referenced to the ferrocene/ferrocenium couple.

PMMA Film Fabrication

A solution of PMMA (98 mg, 35 kDa) in dichloromethane (1.0 mL) was prepared at room temperature in a nitrogen-filled glovebox. Then, the respective iridium complex (2 mg, 2 wt%) was added to the solution and stirred until a homogeneous solution was given. The resulting solution was then drop-coated on a quartz substrate and dried at room temperature overnight.

X-ray Crystallography Details

Single crystals of **Ir-btp-L^1**, **Ir-btp-L^2**, **Ir-piq-L^6**, **Ir-piq-L^{3}H-B**, **Ir-pphen-L^5-B**, and **Ir-piq-L^8** were grown by vapor diffusion of pentane or diethyl ether vapor into concentrated THF or

CH_2Cl_2 solutions. Crystals were mounted on a Bruker Apex II three-circle diffractometer using MoKα radiation (λ = 0.71073 Å). The data were collected at 123(2) K and processed and refined within the APEXII software. Structures were solved by using intrinsic phasing in SHELXT and refined by standard difference Fourier techniques in the SHELXL program.[7] All non-hydrogen atoms were refined with anisotropic displacement parameters. Hydrogen atoms bonded to carbon were fixed in calculated positions using the standard riding model and were refined isotropically. The structures of **Ir-btp-L^1** and **Ir-pphen-L^5-B** included heavily disordered solvent electron density that could not be modeled, necessitating the use of the SQUEEZE command in PLATON.[8] In the structure of **Ir-pphen-L^5-B**, disorder was observed in one of the cyclometalating ligands and in the solvent molecules. All disordered parts were restrained with distance restraints (SADI in SHELX) and rigid-bond restraints (SIMU and DELU in SHELX). The crystals of **Ir-piq-L^{3}H-B** were extremely small and weakly diffracting. The crystal dimension was 0.07×0.05×0.01 mm, and the crystal diffracted poorly at high resolution, leading to some significant level A and level B checkCIF errors after refinement. As a result, the structural metrics (bond distances and bond lengths) in **Ir-piq-L^{3}H-C** are not very reliable and the CIF file was not deposited in CCDC, but the final refined model conclusively confirms the proposed molecular structure.

Synthesis

General procedure for preparation of salicylaldimine complexes. The chloro-bridged cyclometalated iridium dimer was treated with 5 equivalents of Na_2CO_3 in 10 mL of ethanol and stirred for 1h, then 2.1 equivalents of the salicylaldimine ligand (**L^{N}H)** were added. The reaction mixture was refluxed overnight. After the solvent was removed under vacuum, the residue was re-dissolved in CH_2Cl_2 and then filtered through a thin neutral alumina oxide layer, using CH_2Cl_2 as the eluent to flush out the product.

Preparation of [Ir(btp)$_2$L^1] (Ir-btp-L^1). Prepared by the general procedure using [Ir(btp)$_2$(μ-Cl)]$_2$ (100 mg, 0.077 mmol) and **L^{1}H** (27 mg, 0.17 mmol). The resulting crude product was further purified by recrystallization from CH_2Cl_2/pentane to give a red solid. Yield: 67 mg, 56%. ^{1}H NMR (600 MHz, CD_2Cl_2) δ 8.76 (d, J = 5.8 Hz, 1H, btp Ar*H*), 8.43 (d, J = 7.2 Hz, 1H, Ar*H*), 8.02 (s, 1H, N=C*H*Ar), 7.78 (t, J = 7.9 Hz, 1H, Ar*H*), 7.73 (t, J = 7.7 Hz, 1H, Ar*H*), 7.65 (d, J = 8.0 Hz, 2H, Ar*H*), 7.59 (d, J = 8.1 Hz, 1H, Ar*H*), 7.18 (t, J = 8.7 Hz, 1H, Ar*H*), 7.12 – 7.03 (m, 2H, Ar*H*), 7.01 (t, J = 6.6 Hz, 1H, Ar*H*), 6.92 (dd, J = 15.8, 7.3 Hz, 2H, Ar*H*), 6.83 (t, J = 7.6 Hz, 1H, Ar*H*), 6.78 (t, J = 7.7 Hz, 1H, Ar*H*), 6.60 (d, J = 8.6 Hz, 1H, Ar*H*), 6.54 (d, J = 8.1 Hz, 1H, Ar*H*), 6.39 (t, J = 7.7 Hz, 1H, Ar*H*), 6.29 (d, J = 8.1 Hz, 1H, Ar*H*), 6.01 (d, J = 8.2 Hz, 1H, Ar*H*), 3.13 – 3.02 (m, 2H, C*H*$_2$CH$_2$CH$_3$), 1.21 – 1.10 (m, 1H, CH$_2$C*H*$_2$CH$_3$), 1.07 – 0.95 (m, 1H, CH$_2$C*H*$_2$CH$_3$), 0.15 (t, J = 7.3 Hz, 3H, CH$_2$CH$_2$C*H*$_3$). ^{13}C{^{1}H} NMR (151 MHz, CD_2Cl_2) δ 166.3, 166.1, 165.1, 161.8, 151.3, 150.3, 150.0, 148.9, 147.1, 146.7, 142.8, 142.6, 138.5, 138.4, 136.6, 135.4, 135.2, 134.2, 125.8, 125.5, 125.4, 125.1, 124.7, 124.1, 124.0, 123.6, 123.1, 123.0, 120.8, 119.7, 119.6, 119.2, 118.3, 113.7, 66.4, 24.6, 11.5. HRMS-ESI (*m/z*): $[M+H]^+$ calcd for $C_{36}H_{28}IrN_3OS_2$, 776.1374; found, 776.1158.

Preparation of [Ir(btp)$_2$L^2] (Ir-btp-L^2). Prepared by the general procedure using [Ir(btp)$_2$(μ-Cl)]$_2$ (100 mg, 0.077 mmol) and **L$_2$H** (34 mg, 0.16 mmol). The resulting crude product was further purified by recrystallization from CH_2Cl_2/pentane to give a red solid. Yield: 83 mg, 65%. ^{1}H NMR (600 MHz, $CDCl_3$) δ 8.92 (d, J = 5.5 Hz, 1H, btp Ar*H*), 8.79 (d, J = 5.5 Hz, 1H, Ar*H*),

7.91 (s, 1H, N=C*H*Ar), 7.43 – 7.37 (m, 1H, Ar*H*), 7.29 (d, J = 7.8 Hz, 1H, Ar*H*), 7.22 (s, 1H, Ar*H*), 7.12 – 7.11 (m, 1H, Ar*H*), 7.06 (ddd, J = 8.8, 6.8, 1.9 Hz, 1H, Ar*H*), 6.97 – 6.93 (m, 2H, Ar*H*), 6.83 – 6.71 (m, 7H, Ar*H*), 6.67 (d, J = 8.0 Hz, 1H, Ar*H*), 6.54 – 6.48 (m, 1H, Ar*H*), 6.34 (ddd, J = 7.9, 6.9, 1.1 Hz, 1H, Ar*H*), 6.28 (d, J = 8.1 Hz, 2H, Ar*H*), 6.06 (tdd, J = 7.3, 5.8, 1.5 Hz, 3H, Ar*H*), 1.83 (s, 3H, ArC*H*$_3$). The poor solubility of this compound precluded $^{13}C\{^1H\}$ NMR analysis. HRMS-ESI (*m/z*): $[M+Na]^+$ calcd for $C_{40}H_{28}IrN_3OS_2$, 846.1194; found, 846.1172.

Preparation of [Ir(pphen)$_2$L^1] (Ir-pphen-L^1). Prepared by the general procedure using [Ir(pphen)$_2$(μ-Cl)]$_2$ (30 mg, 0.020 mmol) and **L$_1$H** (7 mg, 0.043 mmol). The resulting crude product was further purified by recrystallization from CH_2Cl_2/pentane to give a red solid. Yield: 22 mg, 63%. ^1H NMR (600 MHz, CD_2Cl_2) δ 9.46 (d, J = 8.5 Hz, 1H, pphen Ar*H*), 9.08 – 9.02 (m, 2H, Ar*H*), 8.77 (d, J = 8.2 Hz, 1H, Ar*H*), 8.54 (d, J = 8.0 Hz, 1H, Ar*H*), 8.42 (d, J = 8.2 Hz, 1H, Ar*H*), 8.32 (d, J = 8.1 Hz, 1H, Ar*H*), 8.25 (d, J = 8.1 Hz, 1H, Ar*H*), 8.13 (d, J = 7.9 Hz, 1H, Ar*H*), 7.97 (d, J = 8.4 Hz, 1H, Ar*H*), 7.94 (t, J = 7.8 Hz, 1H, Ar*H*), 7.83 (dd, J = 14.5, 7.4 Hz, 2H, Ar*H*), 7.75 (t, J = 7.5 Hz, 1H, Ar*H*), 7.55 (t, J = 7.3 Hz, 1H, Ar*H*), 7.47 (t, J = 7.6 Hz, 1H, Ar*H*), 7.44 (t, J = 7.8 Hz, 1H, Ar*H*), 7.38 (t, J = 7.8 Hz, 1H, Ar*H*), 7.25 (s, 1H, N=C*H*Ar), 7.06 (d, J = 7.7 Hz, 1H, Ar*H*), 7.02 (t, J = 7.7 Hz, 1H, Ar*H*), 6.98 (t, J = 7.3 Hz, 1H, Ar*H*), 6.65 (t, J = 7.4 Hz, 1H, Ar*H*), 6.59 (t, J = 7.3 Hz, 1H, Ar*H*), 6.39 (d, J = 7.3 Hz, 1H, Ar*H*), 6.33 (ddd, J = 8.2, 7.0, 1.5 Hz, 1H, Ar*H*), 6.15 (dd, J = 7.4, 1.3 Hz, 1H, Ar*H*), 5.80 (d, J = 8.4 Hz, 1H, Ar*H*), 5.76 (t, J = 7.3 Hz, 1H, Ar*H*), 3.38 – 3.28 (m, 1H, C*H*$_2$CH$_2$CH$_3$), 3.07 – 2.98 (m, 1H, C*H*$_2$CH$_2$CH$_3$), 0.81 – 0.72 (m, 1H, CH$_2$C*H*$_2$CH$_3$), 0.25 – 0.15 (m, 4H, CH$_2$C*H*$_2$C*H*$_3$). $^{13}C\{^1H\}$ NMR (126 MHz, $CDCl_3$) δ 174.8, 174.6, 168.0, 165.2, 154.3, 153.4, 149.3, 147.8, 146.1, 143.2, 138.1, 134.4, 134.0, 133.8, 132.7, 132.3, 132.2, 131.8, 131.2, 131.0, 130.5, 129.9, 129.5, 129.5, 128.9, 127.7, 127.3, 127.02, 127.00, 126.9, 126.7, 125.8, 125.6, 124.7, 123.5, 123.3, 122.5, 122.4, 122.3, 122.0, 121.4, 121.3, 119.5, 112.4, 61.7, 24.4, 11.4. HRMS-ESI (*m/z*): $[M+Na]^+$ calcd for $C_{48}H_{36}IrN_3O$, 886.2383; found, 886.2364.

Preparation of [Ir(piq)$_2$L^6] (Ir-piq-L^6). Prepared by the general procedure using [Ir(piq)$_2$(μ-Cl)]$_2$ (100 mg, 0.079 mmol) and **L^{6}H** (50 mg, 0.19 mmol). The resulting crude product was further purified by recrystallization from CH_2Cl_2/pentane to give a red solid. Yield: 80 mg, 59%. ^1H NMR (500 MHz, $CDCl_3$) δ 9.00 – 8.95 (m, 1H, piq Ar*H*), 8.87 (d, J = 6.3 Hz, 1H, Ar*H*), 8.75 (d, J = 6.3 Hz, 1H, Ar*H*), 8.53 (d, J = 8.6 Hz, 1H, Ar*H*), 8.17 (d, J = 8.0 Hz, 1H, Ar*H*), 8.06 (s, 1H, Ar*H*), 7.91 (d, J = 8.1 Hz, 1H, Ar*H*), 7.88 – 7.83 (m, 1H, Ar*H*), 7.73 – 7.67 (m, 3H, Ar*H*), 7.66 – 7.59 (m, 2H, Ar*H*), 7.47 (d, J = 6.4 Hz, 1H, Ar*H*), 7.36 (d, J = 6.4 Hz, 1H, Ar*H*), 7.17 (t, J = 8.8 Hz, 1H, Ar*H*), 7.10 (d, J = 6.0 Hz, 1H, Ar*H*), 6.91 (t, J = 6.9 Hz, 1H, Ar*H*), 6.80 (d, J = 8.2 Hz, 2H, Ar*H*), 6.67 (t, J = 6.7 Hz, 1H, Ar*H*), 6.65 – 6.59 (m, 2H, Ar*H*), 6.46 (t, J = 6.8 Hz, 1H, Ar*H*), 6.38 – 6.32 (m, 2H, Ar*H*), 6.24 (d, J = 6.3 Hz, 1H, Ar*H*), 6.13 (d, J = 8.0 Hz, 2H, Ar*H*). $^{13}C\{^1H\}$ NMR (126 MHz, CD_2Cl_2) δ 169.8, 169.1, 167.8, 161.5, 154.8, 154.5, 146.2, 145.8, 141.7, 140.7, 137.0, 136.9, 134.7, 133.2, 130.8, 129.94, 129.93, 129.4, 129.1, 127.8, 127.4, 127.3, 127.2, 126.6, 126.1, 125.3, 125.0, 124.6, 122.7, 121.5, 121.0, 119.8, 113.6. HRMS-ESI (*m/z*): $[M+H]^+$ calcd for $C_{44}H_{29}F_3IrN_3O$, 866.1965; found, 866.1945.

Preparation of [Ir(piq)$_2$L^{3}H][Cl] (Ir-piq-L^{3}H-B). 1 equivalent of [Ir(piq)$_2$(μ-Cl)]$_2$ (100 mg, 0.079 mmol) was mixed with 2.2 equivalents of **L^{3}H** (29 mg, 0.18 mmol) in 10 mL of anhydrous THF and then the reaction mixture was kept at room temperature for 48 h. After the solvent was removed under vacuum, the residue was re-dissolved in CH_2Cl_2 and filtered through Celite. After evaporating the solvent, the resulting crude product was further purified by recrystallization from

CH_2Cl_2/pentane to give a red solid. Yield: 92 mg, 73%. ^{1}H NMR (500 MHz, $CDCl_3$) δ 11.80 (s, 1H, CON*H*), 9.95 (d, J = 8.0 Hz, 1H, Ar*H*), 9.00 – 8.93 (m, 2H, Ar*H*), 8.28 (d, J = 8.0 Hz, 1H, Ar*H*), 8.23 (d, J = 6.6 Hz, 2H, Ar*H*), 8.08 (t, J = 7.8 Hz, 1H, Ar*H*), 7.98 – 7.87 (m, 2H, Ar*H*), 7.80 – 7.73 (m, 4H, Ar*H*), 7.63 (d, J = 5.1 Hz, 1H, Ar*H*), 7.49 (d, J = 6.4 Hz, 1H, Ar*H*), 7.39 (t, J = 7.6 Hz, 1H, Ar*H*), 7.34 (d, J = 6.4 Hz, 1H, Ar*H*), 7.29 (d, J = 6.4 Hz, 1H, Ar*H*), 7.06 (t, J = 7.6 Hz, 1H, Ar*H*), 7.02 (t, J = 7.6 Hz, 1H, Ar*H*), 6.81 (t, J = 7.4 Hz, 1H, Ar*H*), 6.77 (t, J = 7.4 Hz, 1H, Ar*H*), 6.53 (d, J = 7.7 Hz, 1H, Ar*H*), 6.16 (d, J = 7.6 Hz, 1H, Ar*H*), 3.57 – 3.39 (m, 2H, $CH_2CH_2CH_3$), 1.53 – 1.38 (m, 2H, $CH_2CH_2CH_3$), 0.49 (t, J = 7.4 Hz, 3H, $CH_2CH_2CH_3$). ^{13}C{^{1}H} NMR (151 MHz, $CDCl_3$) δ 171.3, 170.0, 168.0, 150.3, 149.5, 149.4, 148.3, 146.7, 145.3, 140.1, 139.9, 139.3, 137.3, 137.2, 133.2, 133.1, 131.7, 131.6, 130.6, 130.5, 130.4, 129.9, 129.5, 128.9, 128.7, 128.6, 127.9, 127.5, 127.2, 126.5, 126.4, 126.3 122.8, 121.6, 121.4, 121.3, 42.9, 22.1, 11.0. HRMS-ESI (*m/z*): $[M–Cl]^+$ calcd for $C_{39}H_{32}ClIrN_4O$, 765.2196; found, 765.2202.

Preparation of [Ir(piq)$_2$L^4-B] (Ir-piq-L^4-B). After 2.5 equivalents of the **L^{4}H** (42 mg, 0.20 mmol) were treated with 3 equivalents of sodium methoxide (13 mg, 0.24 mmol) in 10 mL THF and stirred for 10 min, 1 equivalent of $[Ir(piq)_2(\mu\text{-}Cl)]_2$ (100 mg, 0.079 mmol) was added. The reaction mixture was kept at room temperature overnight. After the solvent was removed under vacuum, the residue was re-dissolved in CH_2Cl_2 and filtered through Celite. After evaporating the solvent, the crude product was purified by column chromatography (silica gel stationary phase and CH_2Cl_2/ethyl acetate gradient eluent). Previously reported **Ir-piq-L^4** is the less polar product that elutes first as the major product, and **Ir-piq-L^4-B** is the more polar product that elutes second from the column. The eluate of the second fraction was concentrated in vacuo to give an orange solid. Yield: 22 mg, 17%. ^{1}H NMR (500 MHz, $CDCl_3$) δ 8.97 (t, J = 8.3 Hz, 2H, Ar*H*), 8.73 (d, J = 6.4 Hz, 1H, Ar*H*), 8.55 (d, J = 7.7 Hz, 1H, Ar*H*), 8.26 (d, J = 8.0 Hz, 1H, Ar*H*), 8.20 (d, J = 8.3 Hz, 1H, Ar*H*), 7.90 – 7.85 (m, 1H, Ar*H*), 7.82 (d, J = 7.5 Hz, 1H, Ar*H*), 7.76 – 7.66 (m, 5H, Ar*H*), 7.53 (d, J = 6.4 Hz, 1H, Ar*H*), 7.49 (d, J = 5.0 Hz, 1H, Ar*H*), 7.38 (d, J = 6.4 Hz, 1H, Ar*H*), 7.34 (d, J = 8.2 Hz, 2H, **L^4** Ar*H*), 7.23 (d, J = 6.6 Hz, 1H, Ar*H*), 7.13 (t, J = 6.4 Hz, 1H, Ar*H*), 7.00 (t, J = 7.5 Hz, 1H, Ar*H*), 6.94 (t, J = 7.8 Hz, 1H, Ar*H*), 6.87 (d, J = 8.1 Hz, 2H, **L^4** Ar*H*), 6.78 (t, J = 7.5 Hz, 1H, Ar*H*), 6.69 (t, J = 7.5 Hz, 1H, Ar*H*), 6.58 (d, J = 7.6 Hz, 1H, Ar*H*), 6.21 (d, J = 7.9 Hz, 1H, Ar*H*), 2.19 (s, 3H, C*H*$_3$). ^{13}C{^{1}H} NMR (101 MHz, $CDCl_3$) δ 170.1, 168.0, 150.1, 149.9, 149.3, 147.7, 146.1, 145.3, 140.2, 140.1, 139.4, 137.29, 137.26, 136.3, 134.0, 133.1, 132.9, 131.8, 131.6, 130.8, 130.6, 130.5, 130.4, 129.9, 129.8, 129.3, 128.8, 128.7, 127.9, 127.6, 127.2, 126.6, 126.4, 126.3, 123.0, 122.1, 121.7, 121.63, 121.57, 21.1. HRMS-ESI (*m/z*): $[M+H]^+$ calcd for $C_{43}H_{31}IrN_4O$, 813.2202; found, 813.2194.

Preparation of [Ir(pphen)$_2$L^5] (Ir-pphen-L^5) and [Ir(pphen)$_2$L^5-B] (Ir-pphen-L^5-B). After 2.5 equivalents of **L^{5}H** (23 mg, 0.086 mmol) were treated with 3 equivalents of sodium methoxide (6 mg, 0.11 mmol) in 10 mL of anhydrous THF and stirred for 10 min, 1 equivalent of $[Ir(pphen)_2(\mu\text{-}Cl)]_2$ (50 mg, 0.034 mmol) was added. The reaction mixture was kept at room temperature overnight. After the solvent was removed under vacuum, the residue was re-dissolved in CH_2Cl_2 and filtered through Celite. After evaporating the solvent, the crude product was purified by column chromatography (silica gel stationary phase and CH_2Cl_2/ethyl acetate gradient eluent). The eluate from each fraction was concentrated in vacuo to give a red solid. The compound **Ir-pphen-L$_5$** is the less polar product that elutes as the first fraction and is the major product. Yield: 20 mg, 61%. ^{1}H NMR (400 MHz, $CDCl_3$) δ 9.48 (d, J = 9.4 Hz, 1H, pphen Ar*H*), 9.02 (d, J = 8.3 Hz, 1H, Ar*H*), 8.64 (d, J = 8.2 Hz, 1H, Ar*H*), 8.54 (d, J = 8.0 Hz, 1H, Ar*H*), 8.44 (t, J = 7.0 Hz, 2H, Ar*H*), 8.28 (d, J = 8.1 Hz, 1H, Ar*H*), 8.22 (d, J = 5.4 Hz, 1H, Ar*H*),

8.02 (d, J = 8.4 Hz, 1H, Ar*H*), 7.94 – 7.86 (m, 2H, Ar*H*), 7.83 – 7.77 (m, 3H, Ar*H*), 7.75 (d, J = 7.9 Hz, 1H, Ar*H*), 7.58 – 7.48 (m, 3H, Ar*H*), 7.43 (qd, J = 8.4, 1.2 Hz, 2H, Ar*H*), 7.15 – 7.05 (m, 2H, Ar*H*), 6.98 – 6.83 (m, 3H, Ar*H*), 6.74 (t, J = 6.8 Hz, 1H, Ar*H*), 6.68 – 6.54 (m, 5H, Ar*H*), 6.44 (d, J = 8.6 Hz, 1H, Ar*H*). $^{13}C\{^{1}H\}$ NMR (151 MHz, $CDCl_3$) δ 173.8, 173.7, 170.8, 157.1, 156.2, 153.3, 148.9, 147.9, 147.6, 145.9, 143.5, 143.1, 137.2, 136.3, 134.1, 133.8, 133.0, 132.6, 132.1, 131.9, 130.8, 129.8, 129.74, 129.70, 129.5, 129.3, 128.2, 127.4, 127.3, 127.2, 126.63, 126.55, 126.52, 126.4, 125.6, 124.9, 124.8, 124.1, 124.0, 123.9, 123.8, 123.6, 123.5, 122.6, 122.4, 122.0, 121.6, 121.1, 120.7. HRMS-ESI (*m/z*): $[M+Na]^+$ calcd for $C_{51}H_{32}IrN_4O$, 989.2050; found, 989.2035.

Ir-pphen-L^5-B is the more polar product that elutes as the second fraction. Yield: 9 mg, 27%. ^{1}H NMR (600 MHz, $CDCl_3$) δ 9.10 (d, J = 8.2 Hz, 1H, Ar*H*), 9.05 (d, J = 8.3 Hz, 1H, Ar*H*), 8.66 – 8.58 (m, 3H, Ar*H*), 8.42 (d, J = 8.2 Hz, 1H, Ar*H*), 8.41 – 8.35 (m, 2H, Ar*H*), 8.26 (d, J = 5.6 Hz, 1H, Ar*H*), 8.17 (d, J = 8.0 Hz, 1H, Ar*H*), 7.96 (t, J = 7.6 Hz, 1H, Ar*H*), 7.87 (t, J = 7.7 Hz, 2H, Ar*H*), 7.80 (t, J = 9.1 Hz, 2H, Ar*H*), 7.67 (d, J = 8.6 Hz, 1H, Ar*H*), 7.48 (t, J = 7.5 Hz, 1H, Ar*H*), 7.42 – 7.34 (m, 2H, Ar*H*), 7.28 (t, J = 7.8 Hz, 1H, Ar*H*), 7.17 (t, J = 8.8 Hz, 2H, Ar*H*), 7.08 (t, J = 6.4 Hz, 1H, Ar*H*), 7.04 (t, J = 7.5 Hz, 1H, Ar*H*), 7.01 (d, J = 8.1 Hz, 2H, Ar*H*), 6.95 (t, J = 7.8 Hz, 1H, Ar*H*), 6.81 (t, J = 7.4 Hz, 1H, Ar*H*), 6.66 (t, J = 7.4 Hz, 1H, Ar*H*), 6.47 (d, J = 8.1 Hz, 2H, Ar*H*), 6.44 (d, J = 7.6 Hz, 1H, Ar*H*). $^{13}C\{^{1}H\}$ NMR (151 MHz, $CDCl_3$) δ 174.0, 171.8, 166.3, 157.6, 154.7, 153.4, 151.3, 148.3, 147.5, 146.0, 144.2, 143.2, 139.2, 137.1, 136.2, 133.9, 133.7, 132.04, 131.97, 131.7, 131.0, 130.1, 129.7, 129.5, 129.1, 128.9, 127.7, 127.3, 127.2, 126.5, 126.3, 126.0, 125.8, 125.3, 124.9, 124.8, 123.6, 123.2, 122.8, 122.7, 121.6, 121.4, 120.8. HRMS-ESI (*m/z*): $[M+H]^+$ calcd for $C_{51}H_{32}IrN_4O$, 967.2230; found, 967.2241.

Preparation of [Ir(piq)$_2$L^7][PF$_6$] (Ir-piq-L^7). 1 equivalent of $[Ir(piq)_2(\mu\text{-}Cl)]_2$ (100 mg, 0.079 mmol) was dissolved in CH_2Cl_2 and combined with 2.1 equivalents of $AgPF_6$ (42 mg, 0.17 mmol). Then 2.5 equiv of **L^7** (29 mg, 0.20 mmol) was added to the reaction mixture which was stirred at room temperature overnight. The completed reaction mixture was filtered through Celite to remove AgCl. The filtrate volume was reduced, and diethyl ether was added to precipitate the crude product. The solid was dried under vacuum. The resulting crude product was purified by recrystallization from CH_2Cl_2/hexane to give a red solid. Yield: 89 mg, 63%. ^{1}H NMR (500 MHz, CD_2Cl_2) δ 9.27 (s, 1H, Ar*H*), 8.95 (d, J = 7.7 Hz, 1H, Ar*H*), 8.90 (d, J = 9.1 Hz, 1H, Ar*H*), 8.25 (q, J = 7.6 Hz, 3H, Ar*H*), 8.05 (td, J = 7.8, 1.6 Hz, 1H, Ar*H*), 8.00 – 7.93 (m, 2H, Ar*H*), 7.89 (d, J = 6.5 Hz, 1H, Ar*H*), 7.85 – 7.74 (m, 4H, Ar*H*), 7.71 (d, J = 3.9 Hz, 1H, Ar*H*), 7.53 (d, J = 6.4 Hz, 1H, Ar*H*), 7.42 (d, J = 6.4 Hz, 1H, Ar*H*), 7.39 (ddd, J = 7.8, 5.4, 1.4 Hz, 1H, Ar*H*), 7.26 (d, J = 6.4 Hz, 1H, Ar*H*), 7.12 – 7.04 (m, 2H, Ar*H*), 6.89 – 6.79 (m, 2H, Ar*H*), 6.25 (dd, J = 7.7, 1.3 Hz, 1H, Ar*H*), 6.11 (dd, J = 7.6, 1.3 Hz, 1H, Ar*H*), 3.71 – 3.59 (m, 2H, C*H*$_2$CH$_2$CH$_3$), 1.19 – 1.06 (m, 2H, CH$_2$C*H*$_2$CH$_3$), 0.40 (t, J = 7.4 Hz, 3H, CH$_2$CH$_2$C*H*$_3$). $^{13}C\{^{1}H\}$ NMR (126 MHz, CD_2Cl_2) δ 169.2, 169.0, 168.2, 155.5, 152.9, 152.3, 150.7, 145.57, 145.55, 141.1, 140.5, 139.5, 137.1, 132.3, 132.02, 131.95, 131.6, 130.80, 130.76, 130.6, 130.5, 129.6, 129.3, 128.9, 128.8, 127.6, 127.5, 127.00, 126.98, 126.38, 126.35, 122.6, 122.3, 122.1, 121.9, 63.2, 22.6, 10.7. HRMS-ESI (*m/z*): $[M-PF_6]^+$ calcd for $C_{39}H_{32}IrN_4PF_6$, 749.2251; found, 749.2238.

Preparation of [Ir(piq)$_2$L^8] (Ir-piq-L^8). 2.5 equivalents of **L^{8}H** (59 mg, 0.20 mmol) were dissolved in THF and treated with a cold solution of *n*-BuLi (0.10 mL, 2.5 M in *n*-hexane, 0.25 mmol, 3.2 equivalents) at −35 °C for 1h. Then 1 equivalent of $[Ir(piq)_2(\mu\text{-}Cl)]_2$ (100 mg, 0.079

mmol) was added to the reaction mixture and stirred at room temperature overnight. After removing the solvent under vacuum, the residue was extracted with toluene and filtered through Celite. The filtrate was concentrated to about 2 mL, and 2 mL of hexane was added. The mixture was cooled to −35 °C for 2 days to obtain dark red crystals. The cold mixture was filtered, and the product was washed with 4 mL of pentane and dried under vacuum. Yield: 64 mg, 45%. ^{1}H NMR (500 MHz, CD_2Cl_2) δ 9.21 (d, J = 6.3 Hz, 1H, piq Ar*H*), 9.02 (d, J = 6.4 Hz, 1H, Ar*H*), 8.70 (d, J = 8.4 Hz, 1H, Ar*H*), 8.63 (d, J = 8.5 Hz, 1H, Ar*H*), 8.08 (s, 1H, ArN=C*H*Ar), 7.96 (t, J = 8.4 Hz, 2H, **L^{8}** Ar*H*), 7.76 – 7.61 (m, 6H, Ar*H*), 7.53 (d, J = 6.0 Hz, 2H, **L^{8}** Ar*H*), 7.07 (dd, J = 8.1, 1.9 Hz, 1H, Ar*H*), 6.87 (ddd, J = 9.1, 6.5, 1.9 Hz, 1H, Ar*H*), 6.60 – 6.51 (m, 2H, Ar*H*), 6.43 (dd, J = 8.0, 2.2 Hz, 1H, Ar*H*), 6.39 (d, J = 7.4 Hz, 2H, Ar*H*), 6.33 (dd, J = 8.0, 2.3 Hz, 1H, Ar*H*), 6.30 – 6.21 (m, 2H, Ar*H*), 6.07 (d, J = 9.2 Hz, 1H, Ar*H*), 6.05 – 5.97 (m, 5H, Ar*H*), 5.84 (dd, J = 7.7, 1.3 Hz, 1H, Ar*H*), 5.08 (dd, J = 8.0, 2.2 Hz, 1H, Ar*H*), 2.01 (s, 3H, C*H*$_3$), 1.96 (s, 3H, C*H*$_3$). ^{13}C{^{1}H} NMR (126 MHz, CD_2Cl_2) δ 169.82, 169.80, 160.5, 159.6, 159.5, 151.8, 151.5, 149.7, 145.9, 145.0, 142.7, 142.6, 137.1, 136.9, 136.8, 133.51, 133.47, 132.4, 131.9, 130.67, 130.65, 130.5, 129.6, 129.4, 129.0, 128.3, 128.2, 127.7, 127.51, 127.49, 127.2, 127.14, 127.05, 126.7, 126.5, 126.1, 125.4, 125.3, 123.1, 119.8, 119.6, 119.4, 119.3, 118.9, 117.5, 110.1, 20.31, 20.28. HRMS-ESI (*m/z*): $[M+Na]^+$ calcd for $C_{51}H_{39}IrN_4$, 923.2700; found, 923.2691.

Table S1. Summary of X-ray crystallographic data for complexes **Ir-btp-L[1]**, **Ir-btp-L[2]** and **Ir-piq-L[6]**.

	Ir-btp-L[1]	**Ir-btp-L[2]**	**Ir-piq-L[6]**
CCDC	2300731	2300732	2300733
Chemical formula	$C_{36}H_{28}IrN_3OS_2$	$C_{40}H_{28}IrN_3OS_2$	$C_{44}H_{29}F_3IrN_3O$
M_r	774.93	822.97	864.90
Crystal system, space group	Trigonal, $R\bar{3}$:H	Triclinic, $P\bar{1}$	Monoclinic, $P2_1/c$
Temperature (K)	123(2)	123	123
a, b, c (Å)	36.2343 (15), 36.2343 (15), 15.9108 (7)	10.7907 (11), 11.0742 (11), 14.2844 (14)	18.3303 (17), 11.9159 (11), 15.9378 (15)
α, β, γ (°)	90, 90, 120	107.087 (1), 102.368 (1), 93 .397 (1)	90, 106.937 (1), 90
V (Å^3)	18091.0 (17)	1580.0 (3)	3330.2 (5)
Z	18	2	4
μ (mm^{-1})	3.45	4.40	4.07
Crystal size (mm)	0.44 × 0.30 × 0.19	0.17 × 0.14 × 0.09	0.28 × 0.1 × 0.06
T_{min}, T_{max}	0.508, 0.746	0.613, 0.746	0.601, 0.746
No. of measured, independent and observed [$I > 2\sigma(I)$] reflections	31337, 8981, 7614	28181, 7275, 6228	20714, 7708, 6321
R_{int}	0.046	0.066	0.042
$(\sin\theta/\lambda)_{max}$ (Å^{-1})	0.649	0.651	0.651
$R[F^2 > 2\sigma(F^2)]$, $wR(F^2)$, S	0.023, 0.047, 0.95	0.036, 0.070, 1.02	0.031, 0.065, 0.97
No. of reflections	8981	7275	7708
No. of parameters	389	425	469
No. of restraints	0	0	0
	$w = 1/[\sigma^2(F_o^2) + (0.0103P)^2]$ where $P = (F_o^2 + 2F_c^2)/3$	$w = 1/[\sigma^2(F_o^2) + (0.0265P)^2]$ where $P = (F_o^2 + 2F_c^2)/3$	$w = 1/[\sigma^2(F_o^2) + (0.0276P)^2]$ where $P = (F_o^2 + 2F_c^2)/3$
$\Delta\rho_{max}$, $\Delta\rho_{min}$ (e Å^{-3})	1.01, −1.18	0.90, −0.93	0.80, −0.84

Table S2. Summary of X-ray crystallographic data for the complex **Ir-pphen-L^5-B**.

	Ir-pphen-L^5-B·2C_4H_8O
CCDC	2300734
Chemical formula	$C_{51}H_{31}F_3IrN_4O·2(C_4H_8O)$
M_r	1109.20
Crystal system, space group	Triclinic, $P\bar{1}$
Temperature (K)	123
a, b, c (Å)	10.916 (4), 13.168 (4), 18.015 (6)
α, β, γ (°)	82.060 (5), 78.545 (5), 78.258 (5)
V (Å^3)	2472.0 (14)
Z	2
μ (mm^{-1})	2.76
Crystal size (mm)	0.15 × 0.07 × 0.03
T_{min}, T_{max}	0.647, 0.745
No. of measured, independent and observed [$I > 2\sigma(I)$] reflections	32112, 10180, 7894
R_{int}	0.079
$(\sin\theta/\lambda)_{max}$ (Å^{-1})	0.629
$R[F^2 > 2\sigma(F^2)]$, $wR(F^2)$, S	0.049, 0.113, 0.99
No. of reflections	10180
No. of parameters	631
No. of restraints	1291
	$w = 1/[\sigma^2(F_o^2) + (0.0532P)^2]$ where $P = (F_o^2 + 2F_c^2)/3$
$\Delta\rho_{max}$, $\Delta\rho_{min}$ (e Å^{-3})	1.15, −1.48

Table S3. Summary of X-ray crystallographic data for the complex **Ir-piq-L[8]**.

	Ir-piq-L[8]
CCDC	2300735
Chemical formula	$C_{44}H_{32}IrN_3O$
M_r	810.92
Crystal system, space group	Triclinic, $P\bar{1}$
Temperature (K)	123(2)
a, b, c (Å)	9.2199 (4), 13.999 (2), 14.701 (2)
α, β, γ (°)	70.672 (2), 84.198 (2), 74.663 (2)
V (Å^3)	1726.6 (5)
Z	2
μ (mm^{-1})	3.91
Crystal size (mm)	0.30 × 0.21 × 0.14
T_{min}, T_{max}	0.576, 0.746
No. of measured, independent and observed [$I > 2\sigma(I)$] reflections	43010, 7957, 7324
R_{int}	0.044
$(\sin\theta/\lambda)_{max}$ (Å^{-1})	0.651
$R[F^2 > 2\sigma(F^2)]$, $wR(F^2)$, S	0.022, 0.054, 1.04
No. of reflections	7957
No. of parameters	443
No. of restraints	0
	$w = 1/[\sigma^2(F_o^2) + (0.0312P)^2]$ where $P = (F_o^2 + 2F_c^2)/3$
$\Delta\rho_{max}$, $\Delta\rho_{min}$ (e Å^{-3})	1.39, −0.41

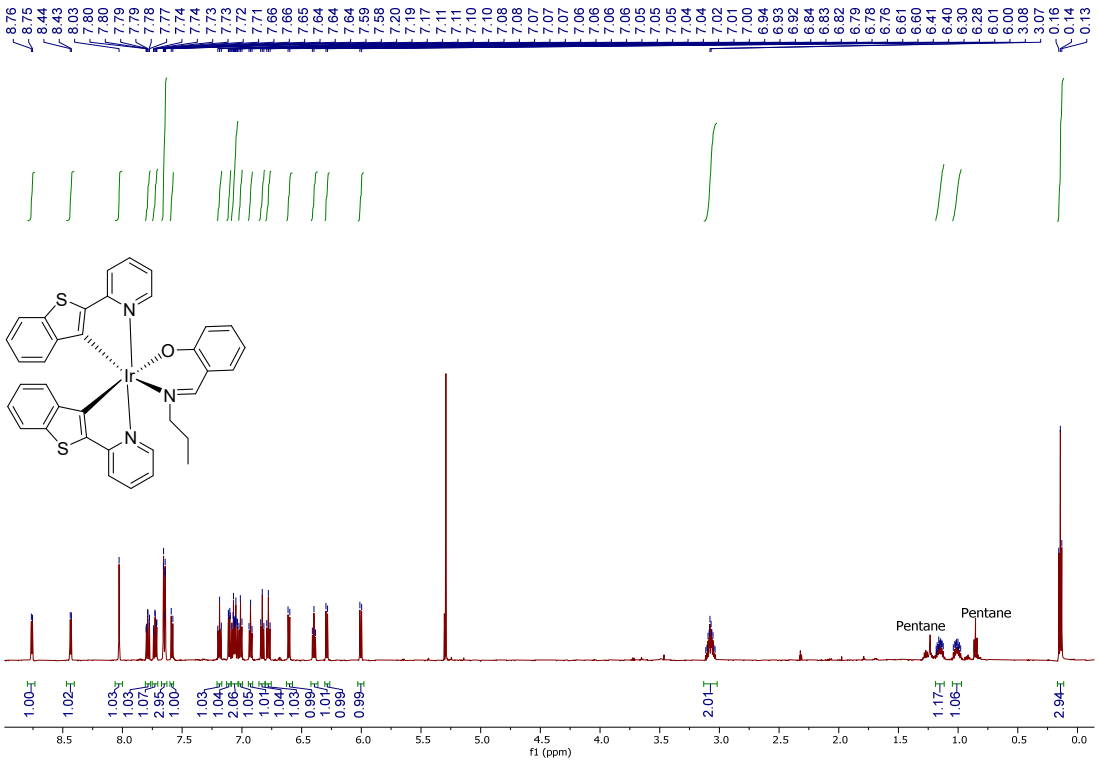

Fig. S1. ^{1}H NMR spectrum of **Ir-btp-L^{1}**, recorded in methylene chloride-d_2 at 600 MHz.

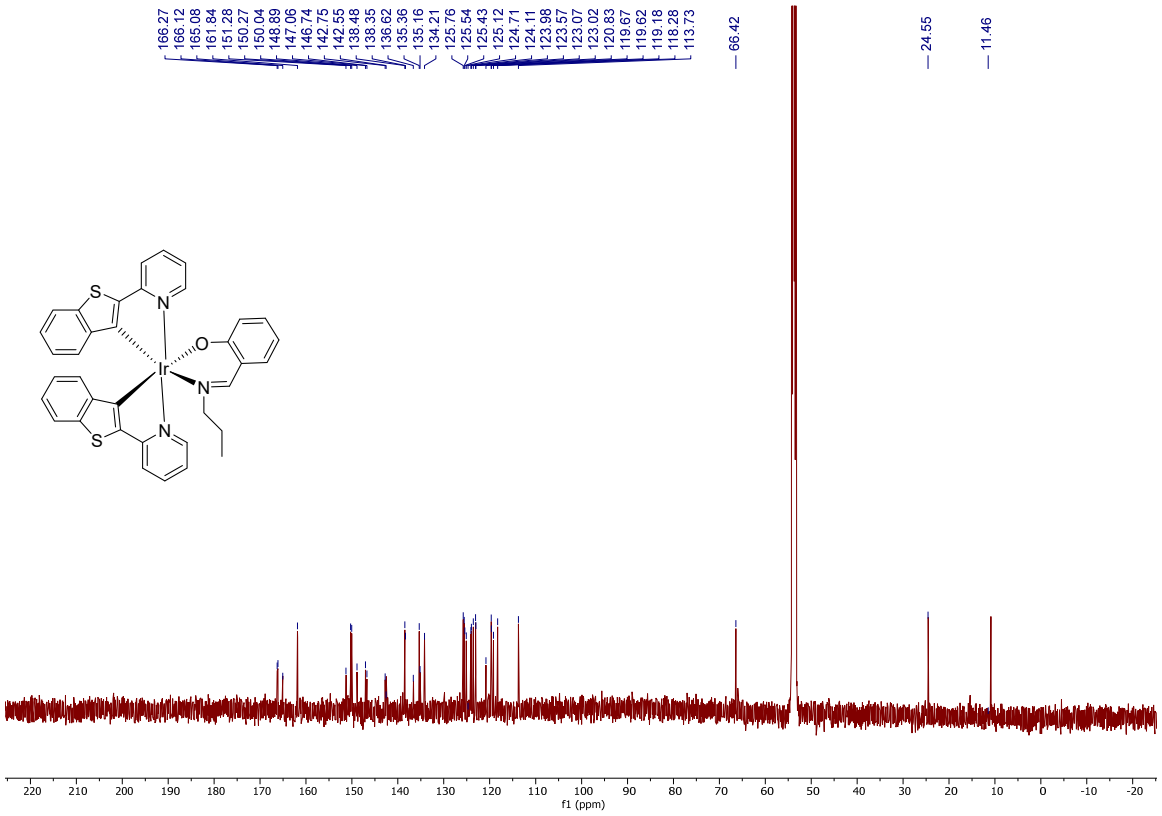

Fig. S2. ^{13}C{^{1}H} NMR spectrum of **Ir-btp-L^{1}**, recorded in methylene chloride-d_2 at 151 MHz.

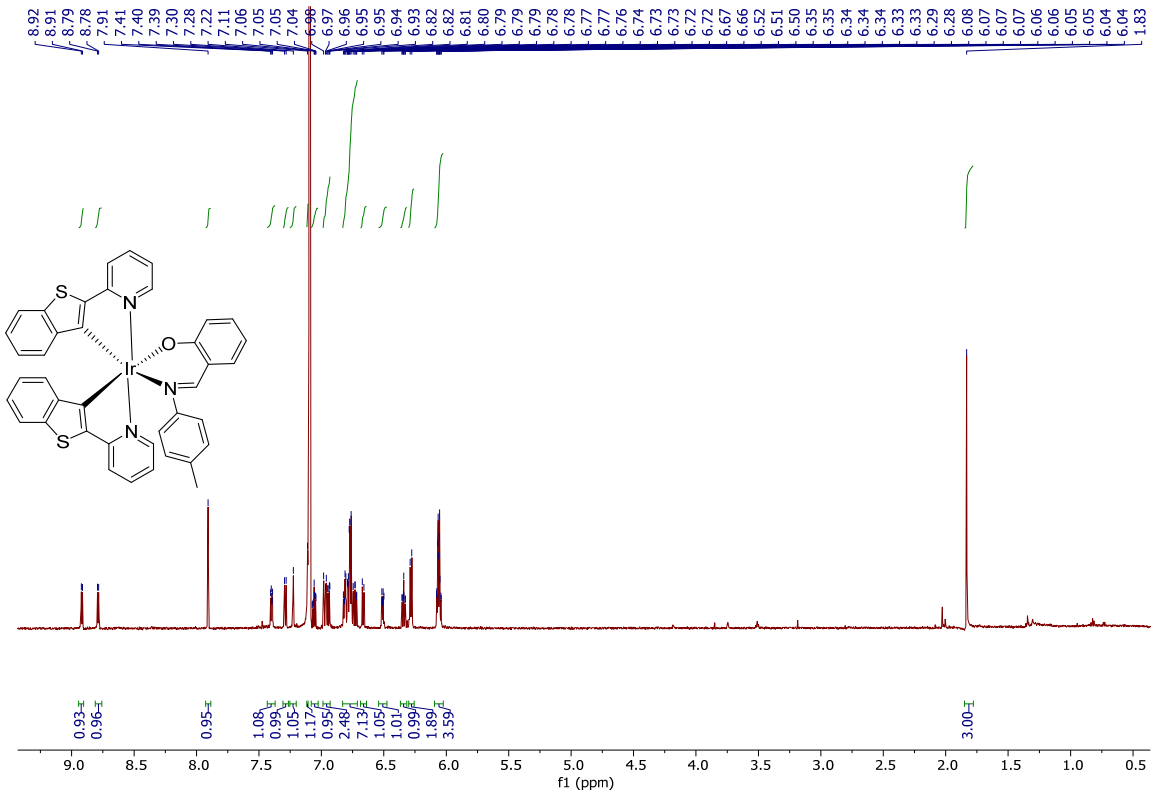

Fig. S3. [1]H NMR spectrum of **Ir-btp-L[2]**, recorded in in chloroform-*d* at 600MHz.

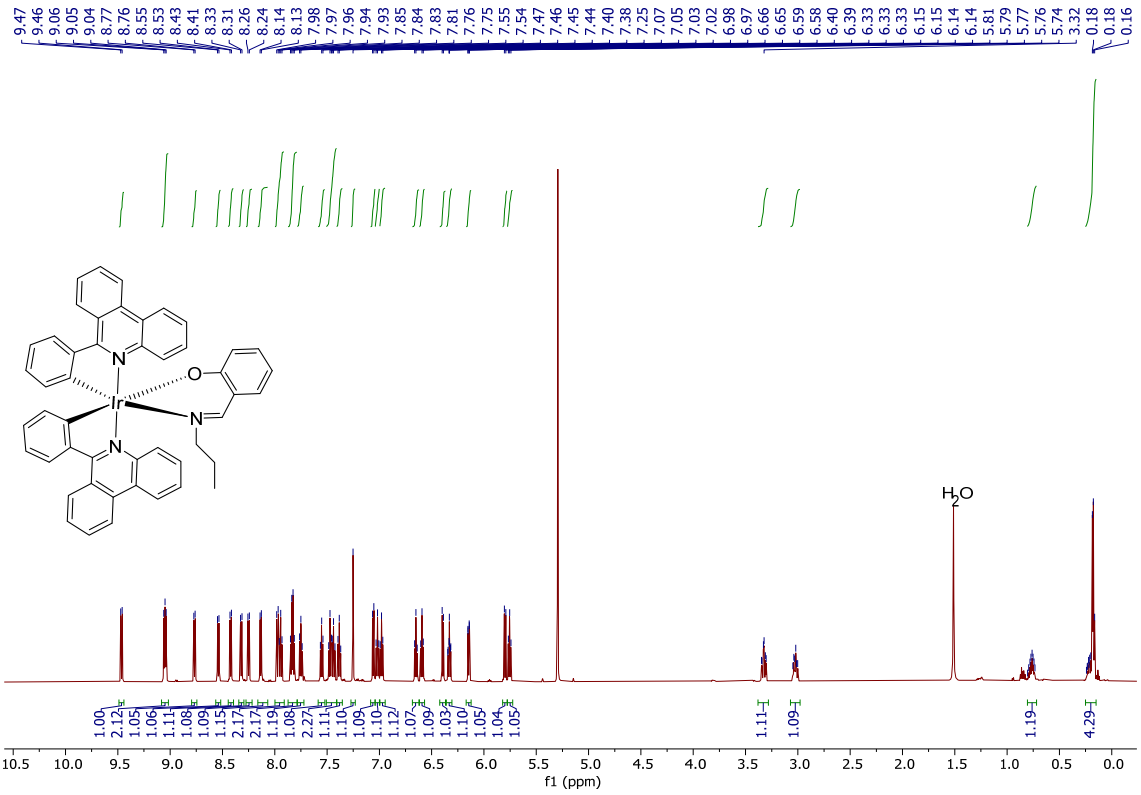

Fig. S4. [1]H NMR spectrum of **Ir-pphen-L[1]**, recorded in methylene chloride-d_2 at 600 MHz.

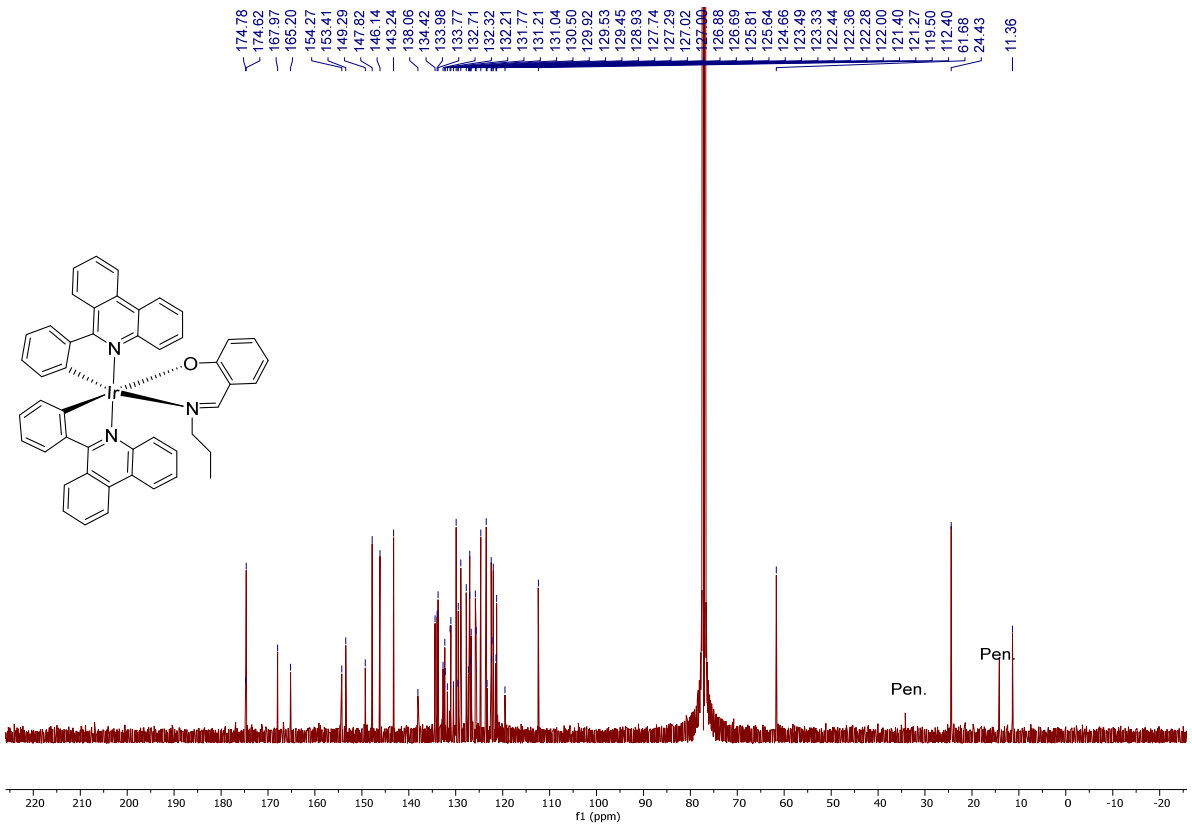

Fig. S5. $^{13}C\{^{1}H\}$ NMR spectrum of **Ir-pphen-L[1]**, recorded in chloroform-*d* at 151 MHz.

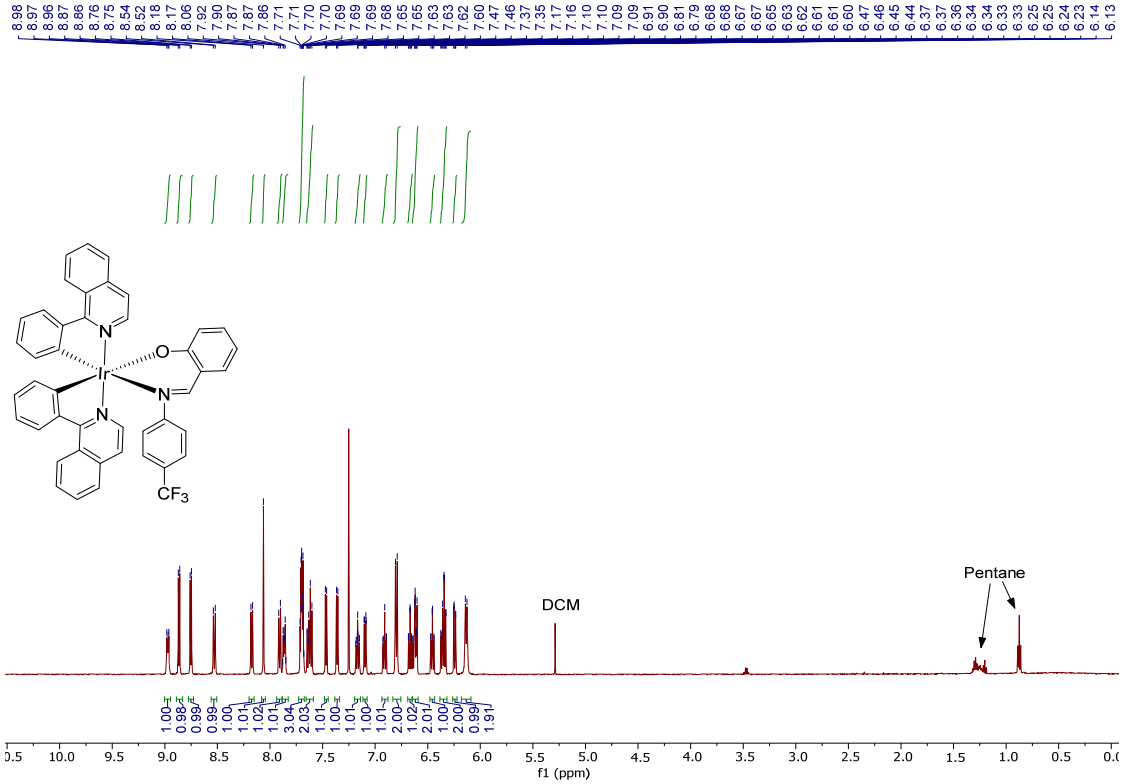

Fig. S6. ^{1}H NMR spectrum of **Ir-piq-L[6]**, recorded in chloroform-*d* at 500 MHz.

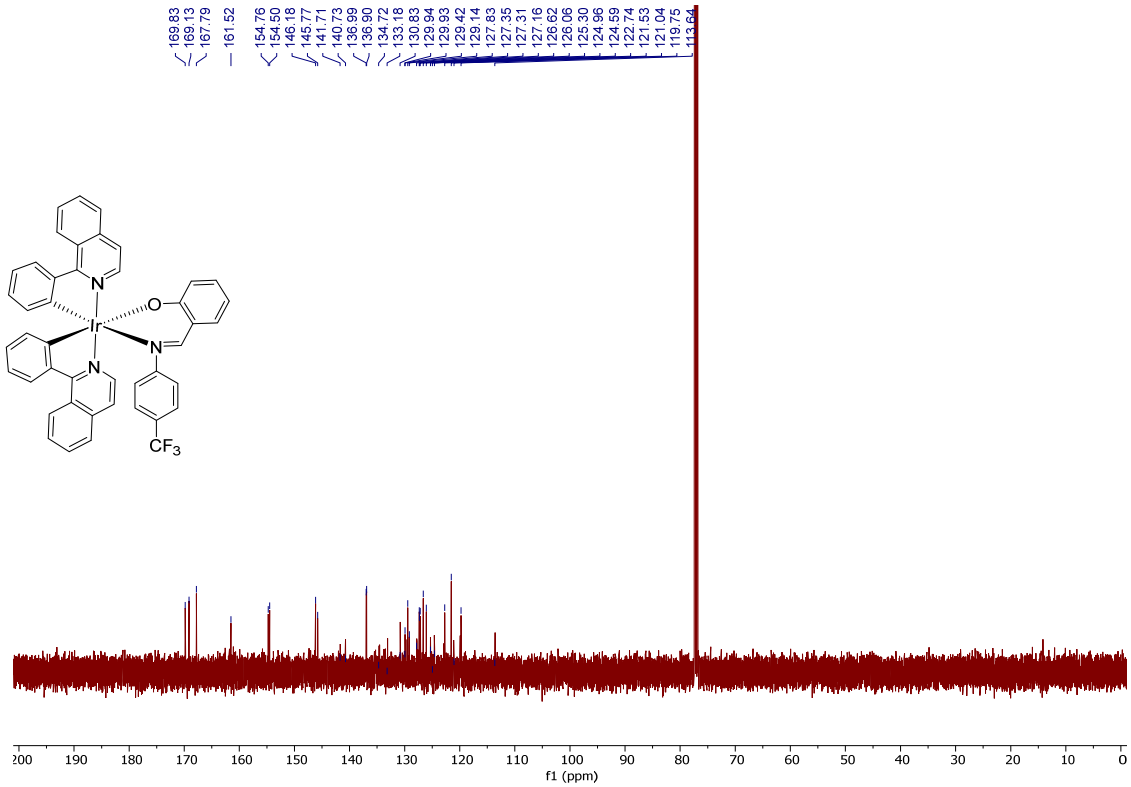

Fig. S7. $^{13}C\{^{1}H\}$ NMR spectrum of **Ir-piq-L^{6}**, recorded in methylene chloride-d_2 at 151 MHz.

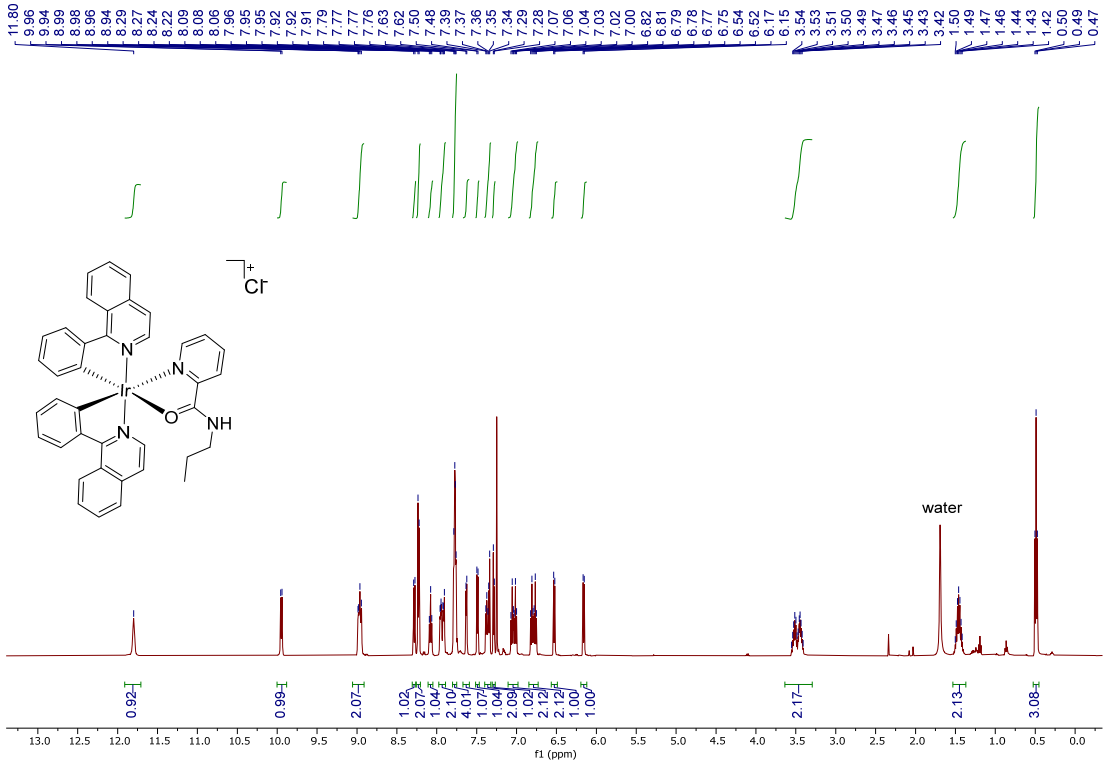

Fig. S8. ^{1}H NMR spectrum of **Ir-piq-L^{3}H-B**, recorded in chloroform-*d* at 500 MHz.

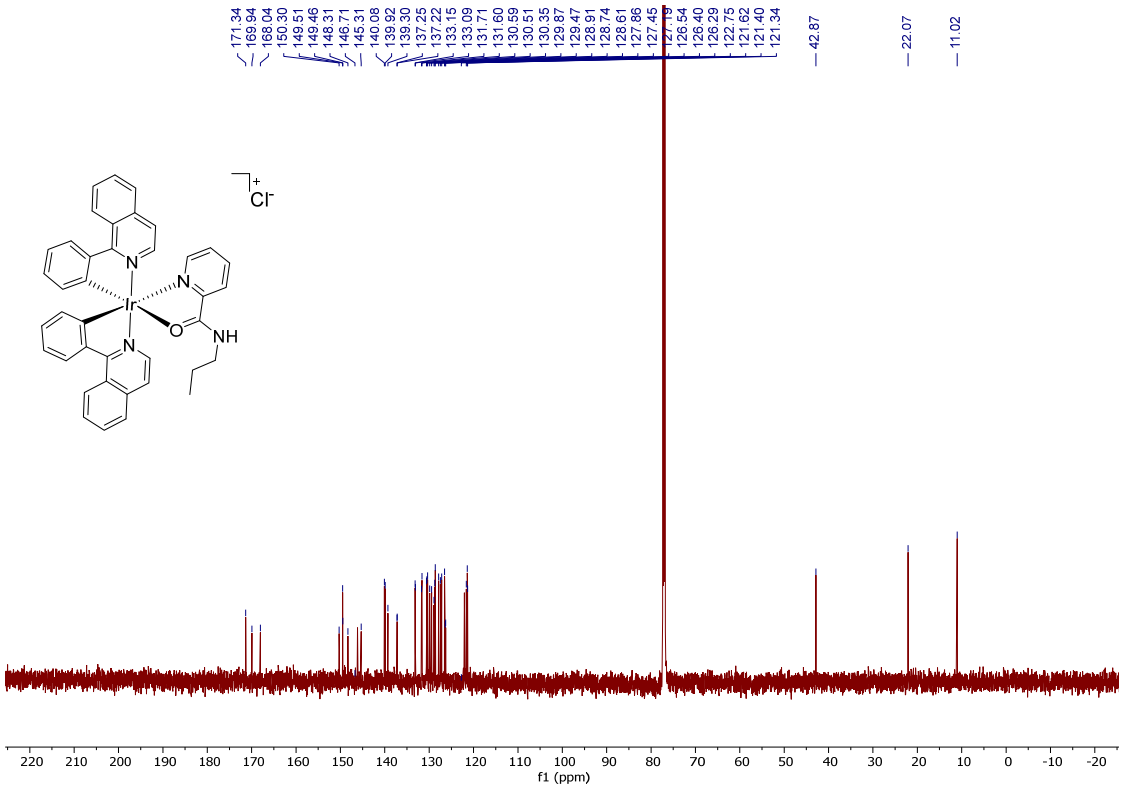

Fig. S9. $^{13}C\{^{1}H\}$ NMR spectrum of **Ir-piq-L^{3}H-B**, recorded in chloroform-*d* at 151 MHz.

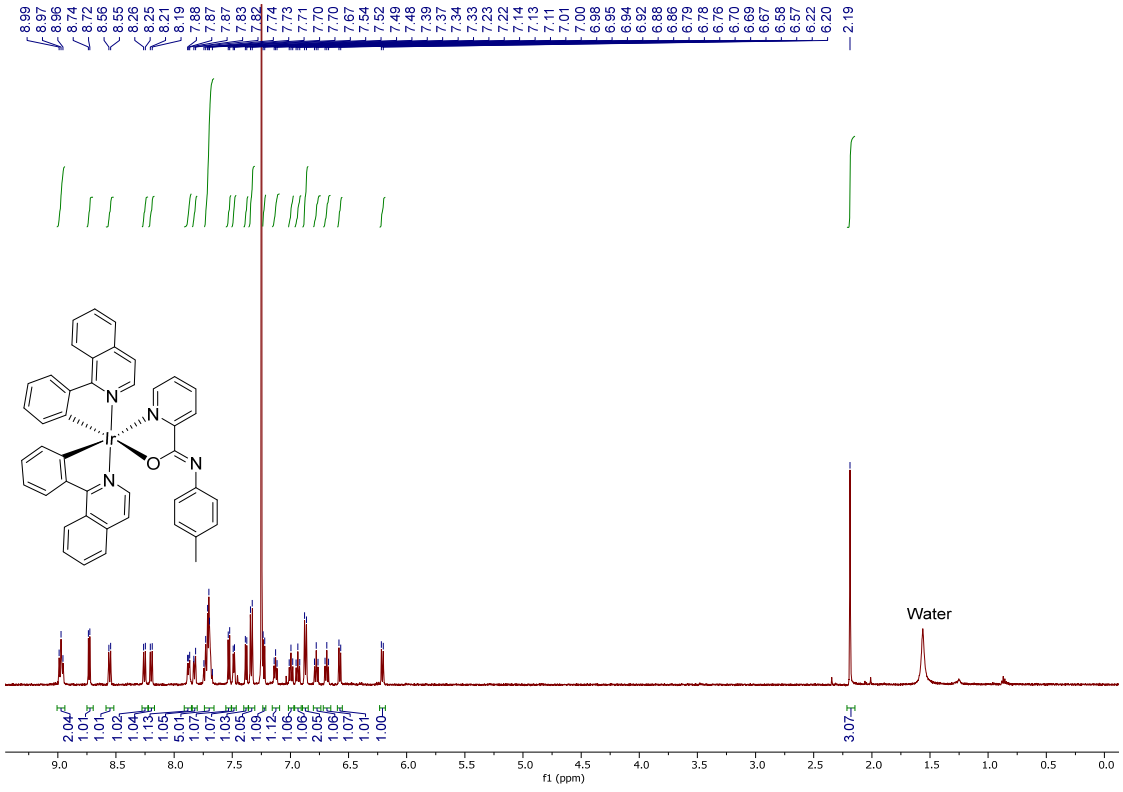

Fig. S10. ^{1}H NMR spectrum of **Ir-piq-L^{4}-B**, recorded in chloroform-*d* at 500 MHz.

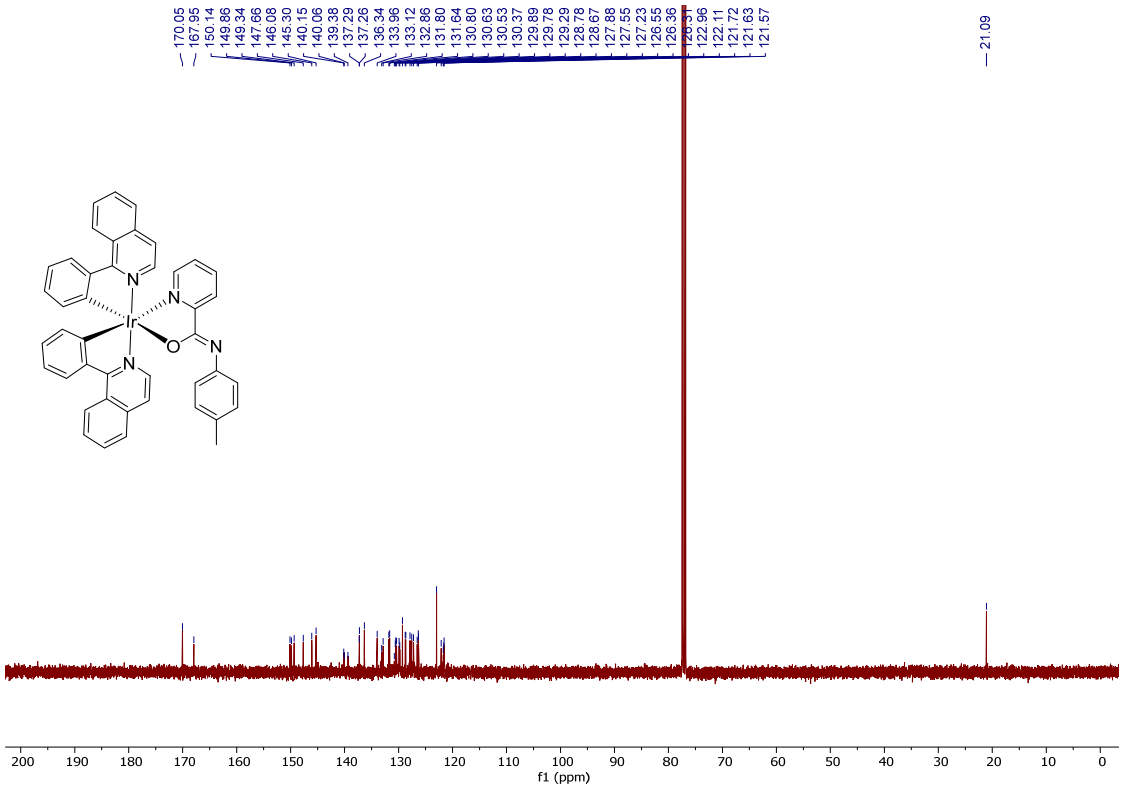

Fig. S11. $^{13}C\{^{1}H\}$ NMR spectrum of **Ir-piq-L^{4}-B**, recorded in chloroform-*d* at 101 MHz.

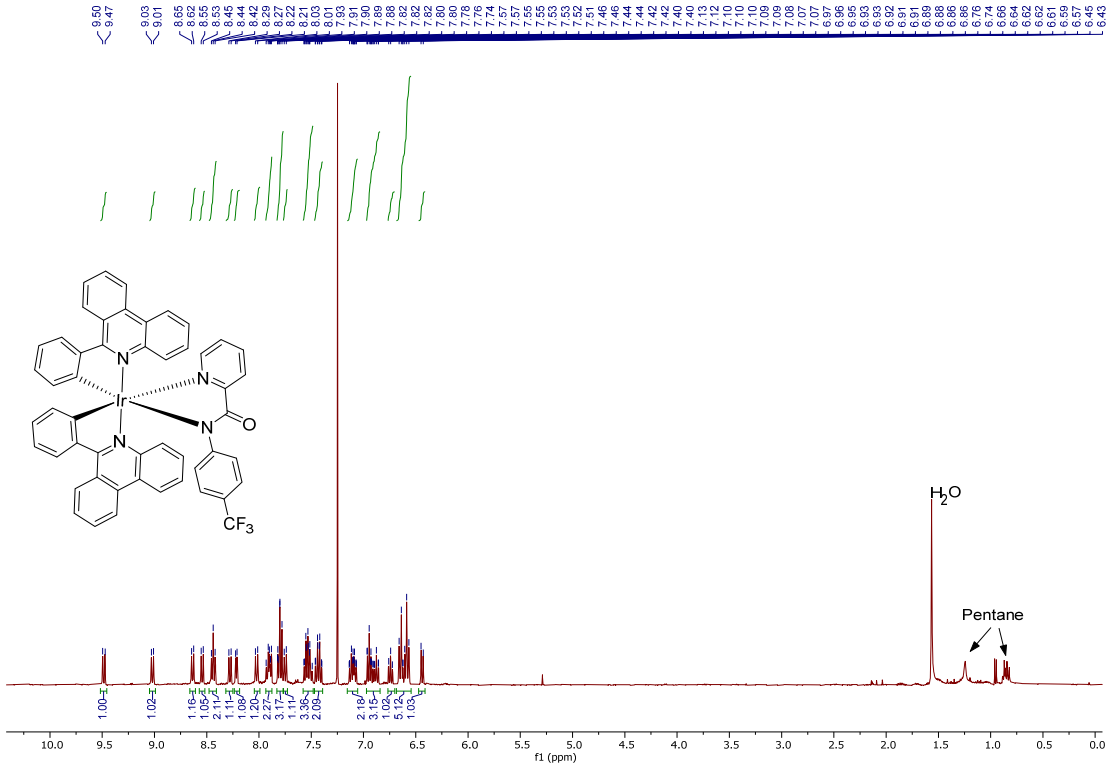

Fig. S12. ^{1}H NMR spectrum of **Ir-pphen-L^{5}**, recorded in chloroform-*d* at 400 MHz.

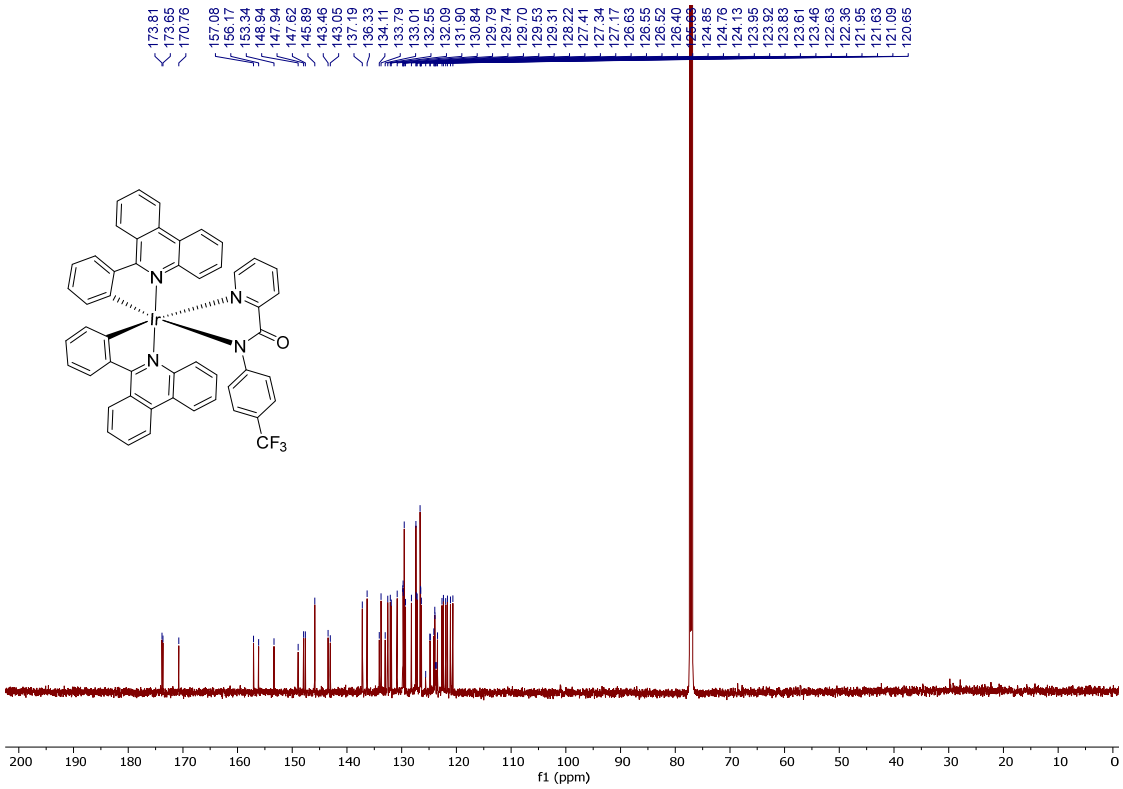

Fig. S13. $^{13}C\{^{1}H\}$ NMR spectrum of **Ir-pphen-L^5**, recorded in chloroform-*d* at 151 MHz.

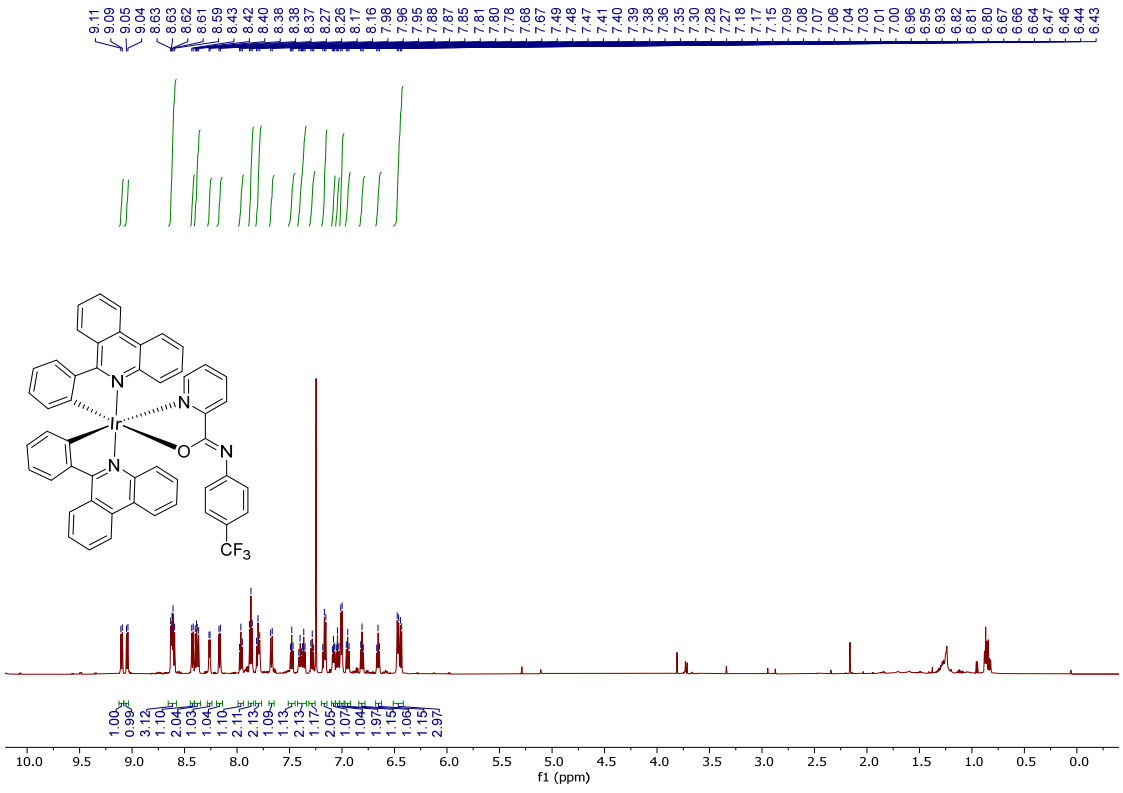

Fig. S14. ^{1}H NMR spectrum of **Ir-pphen-L^5-B**, recorded in chloroform-*d* at 600 MHz.

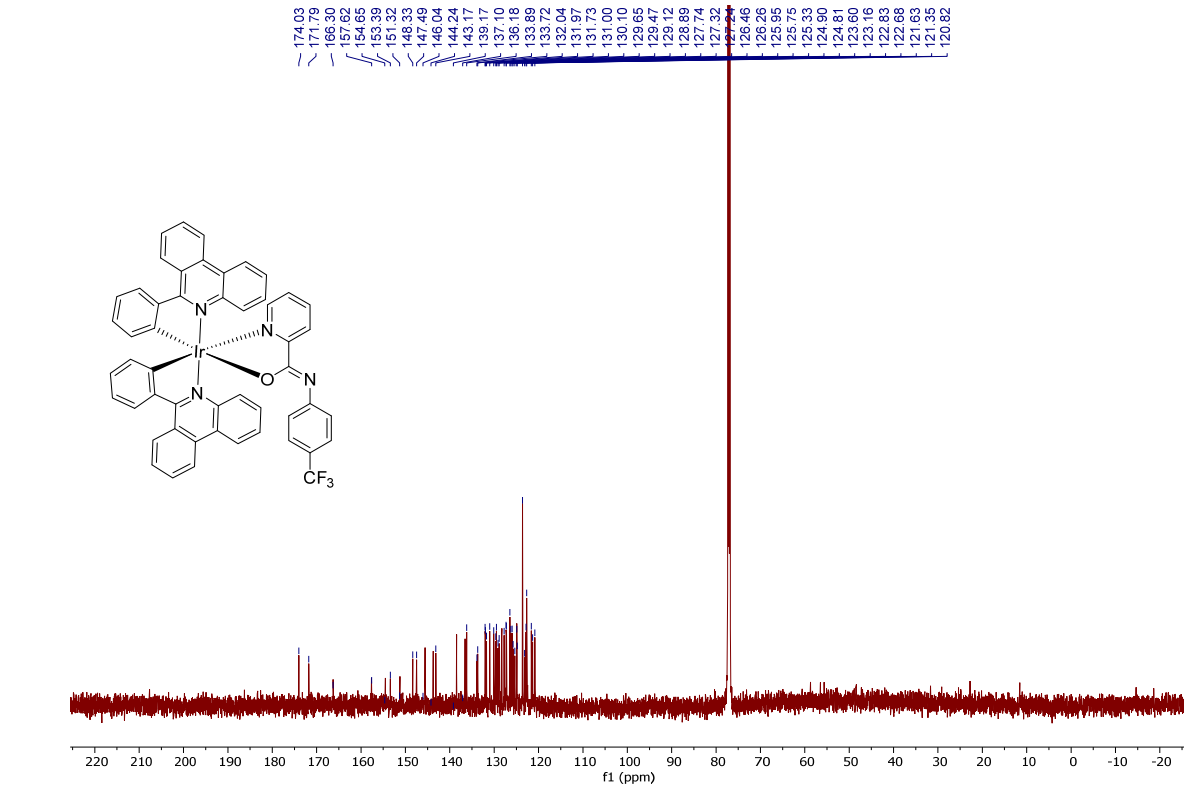

Fig. S15. $^{13}C\{^{1}H\}$ NMR spectrum of **Ir-pphen-L^{5}-B**, recorded in chloroform-*d* at 151 MHz.

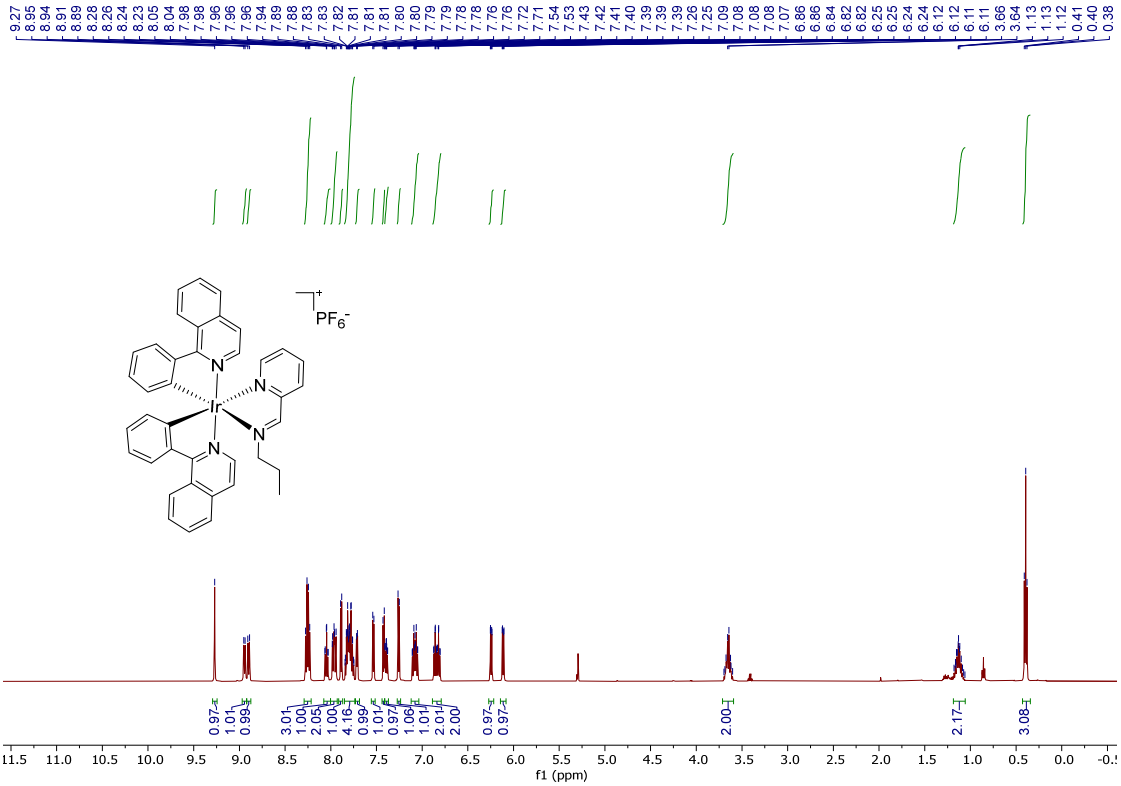

Fig. S16. ^{1}H NMR spectrum of **Ir-piq-L^{7}**, recorded in methylene chloride-d_2 at 500 MHz.

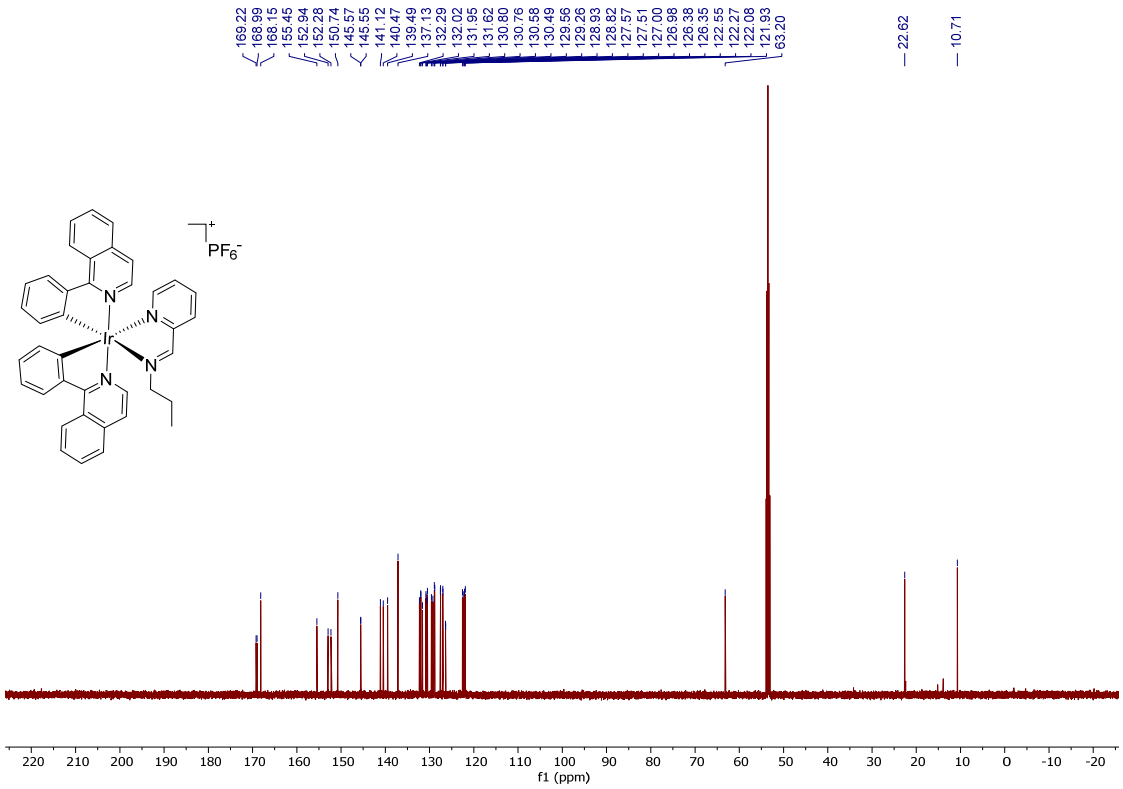

Fig. S17. $^{13}C\{^{1}H\}$ NMR spectrum of **Ir-piq-L**[7], recorded in methylene chloride-*d*2 at 126 MHz.

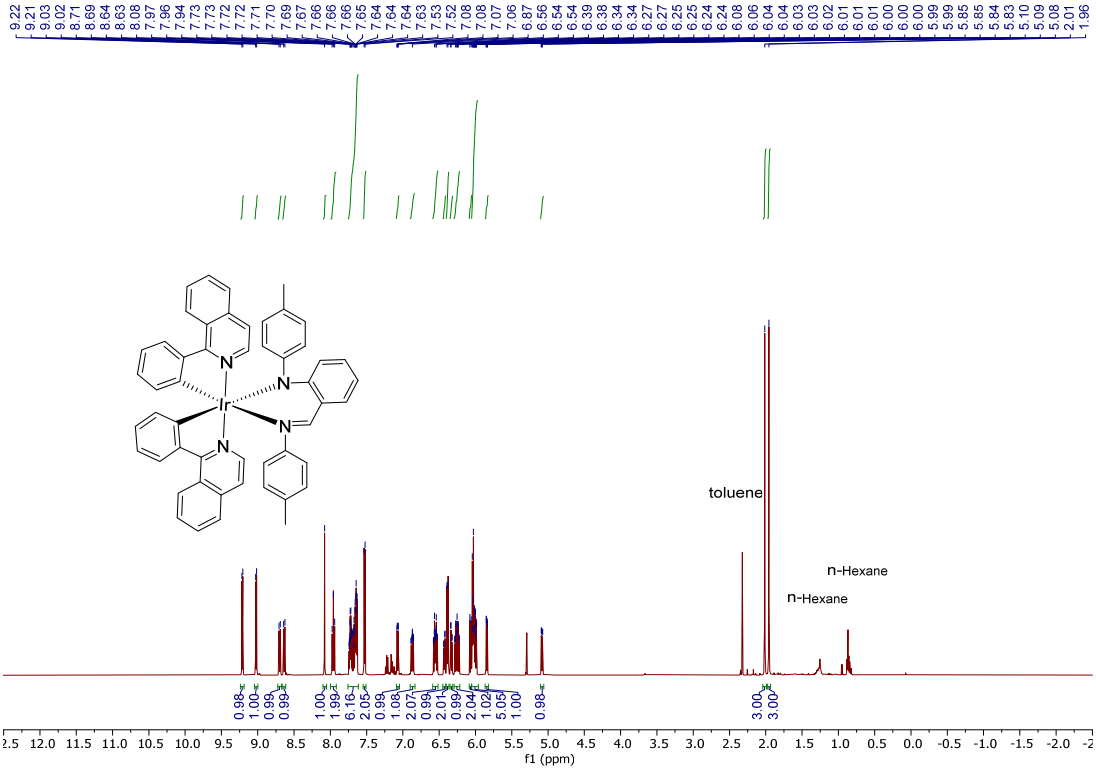

Fig. S18. ^{1}H NMR spectrum of **Ir-piq-L**[8], recorded in methylene chloride-*d*2 at 500 MHz.

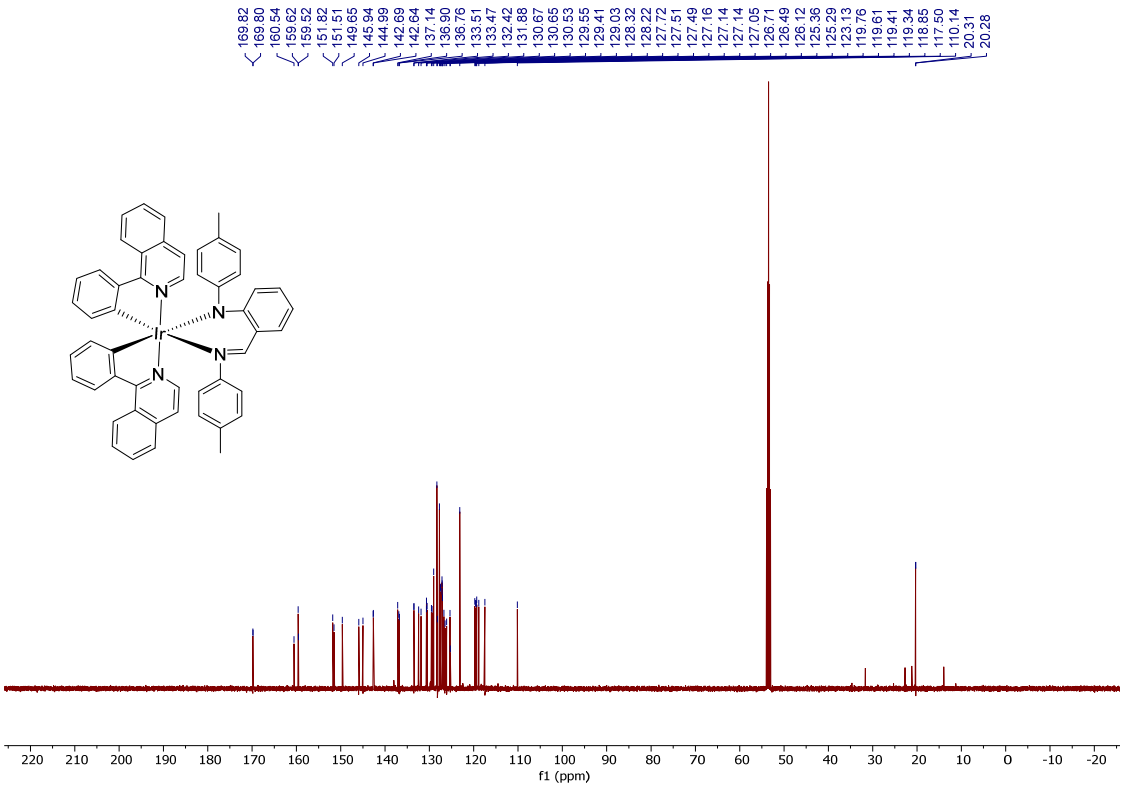

Fig. S19. $^{13}C\{^{1}H\}$ NMR spectrum of **Ir-piq-L[8]**, recorded in methylene chloride-*d*$_2$ at 126 MHz.

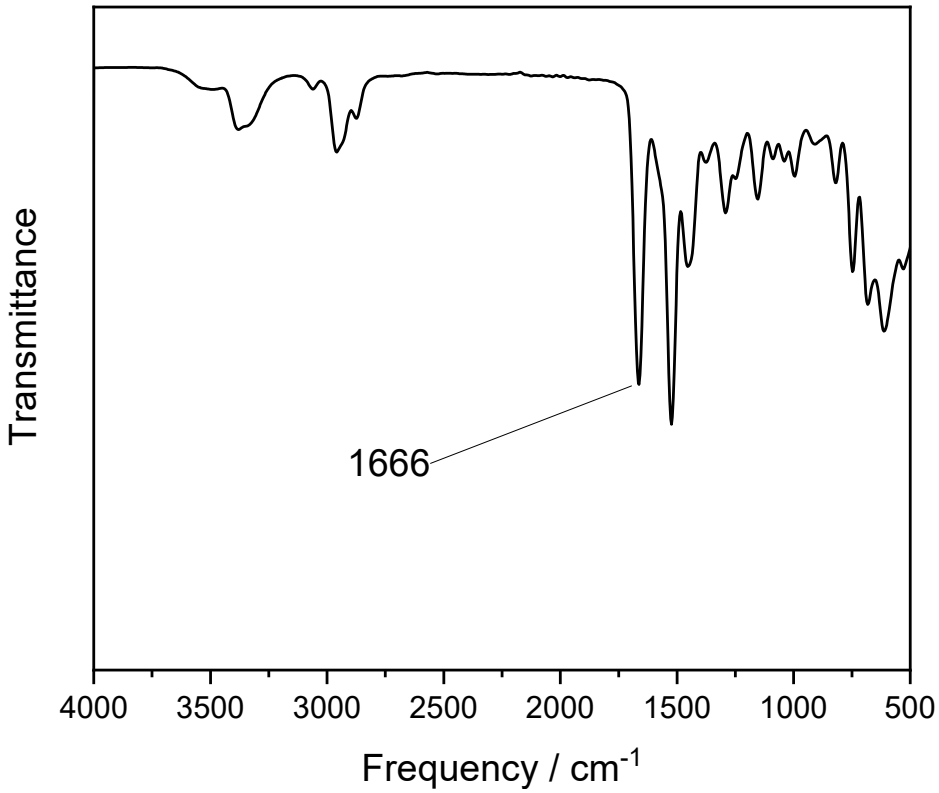

Fig. S20. FTIR spectrum of free ligand $\mathbf{L^3H}$.

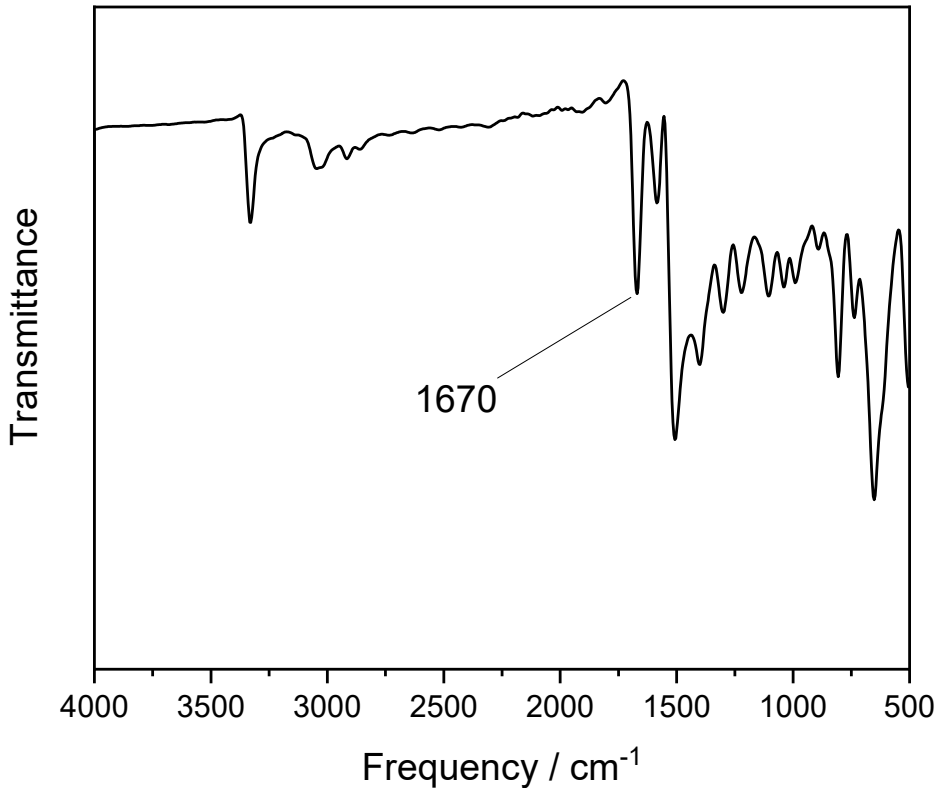

Fig. S21. FTIR spectrum of free ligand $\mathbf{L^4H}$.

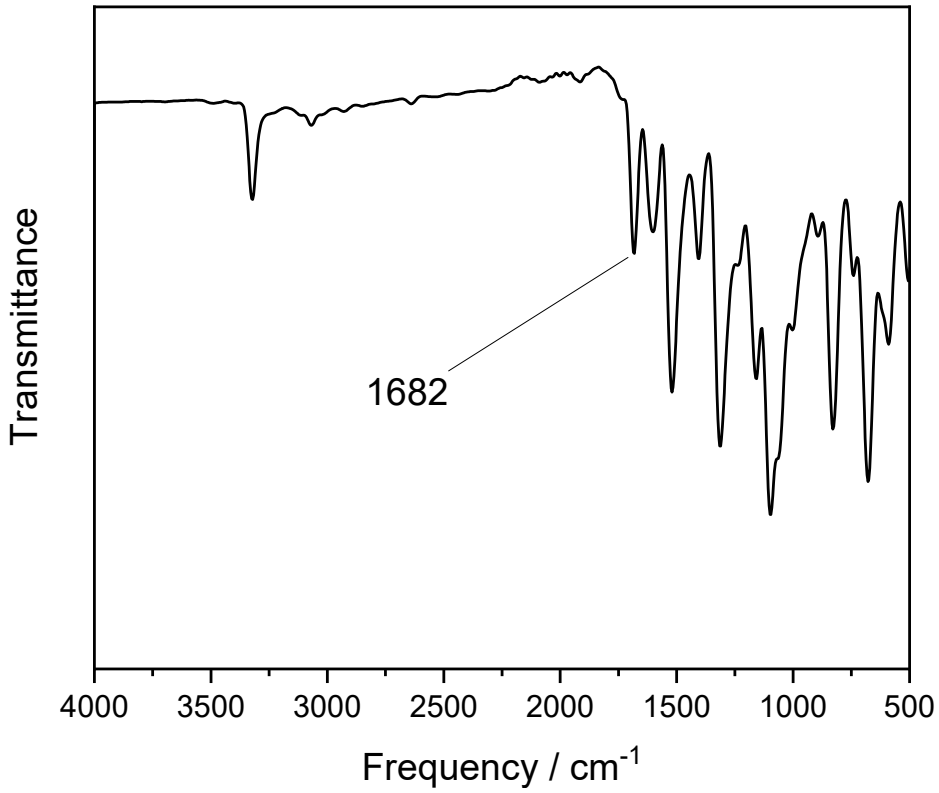

Fig. S22. FTIR spectrum of free ligand $\mathbf{L^5H}$.

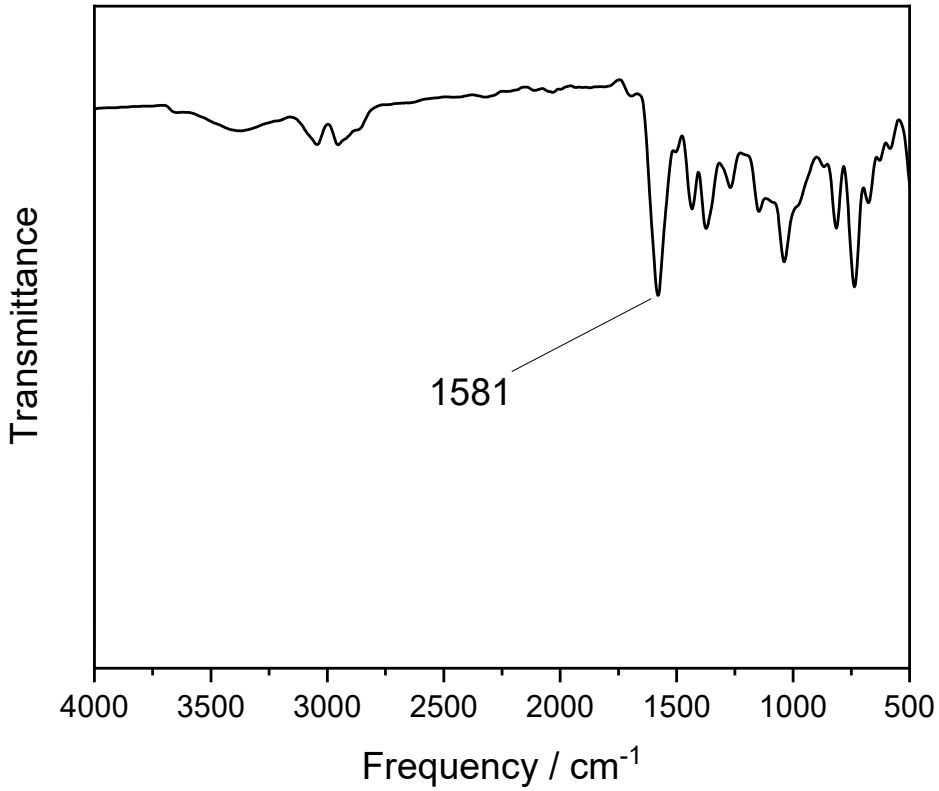

Fig. S23. FTIR spectrum of complex **Ir-piq-$\mathbf{L^3}$**.

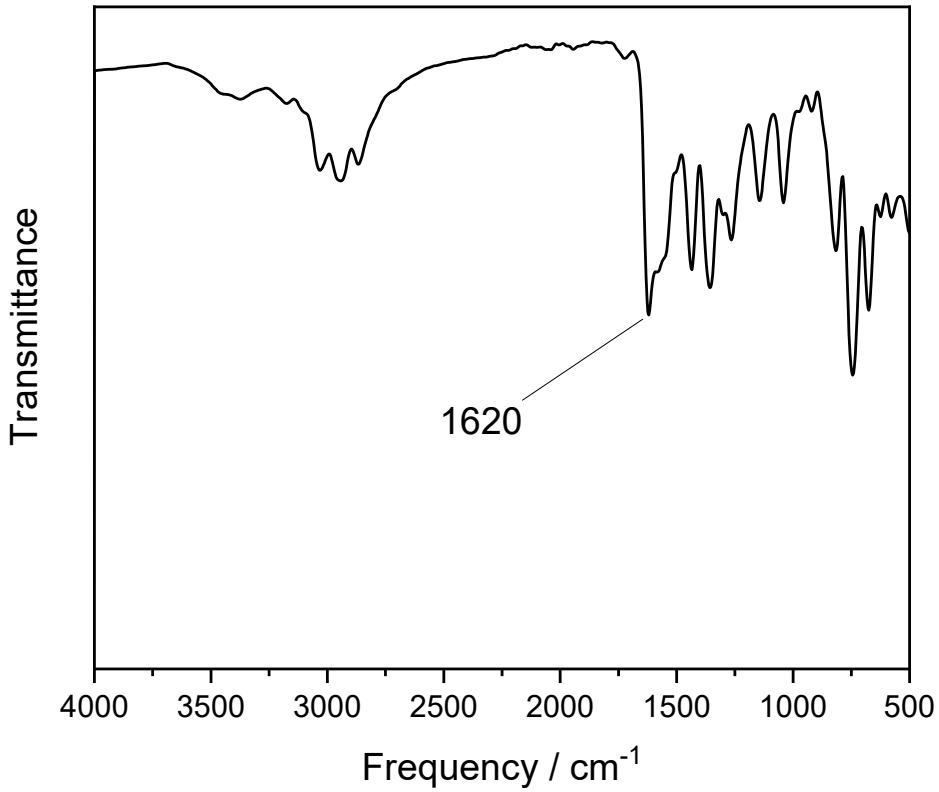

Fig. S24. FTIR spectrum of complex **Ir-piq-L^{3}H-B**.

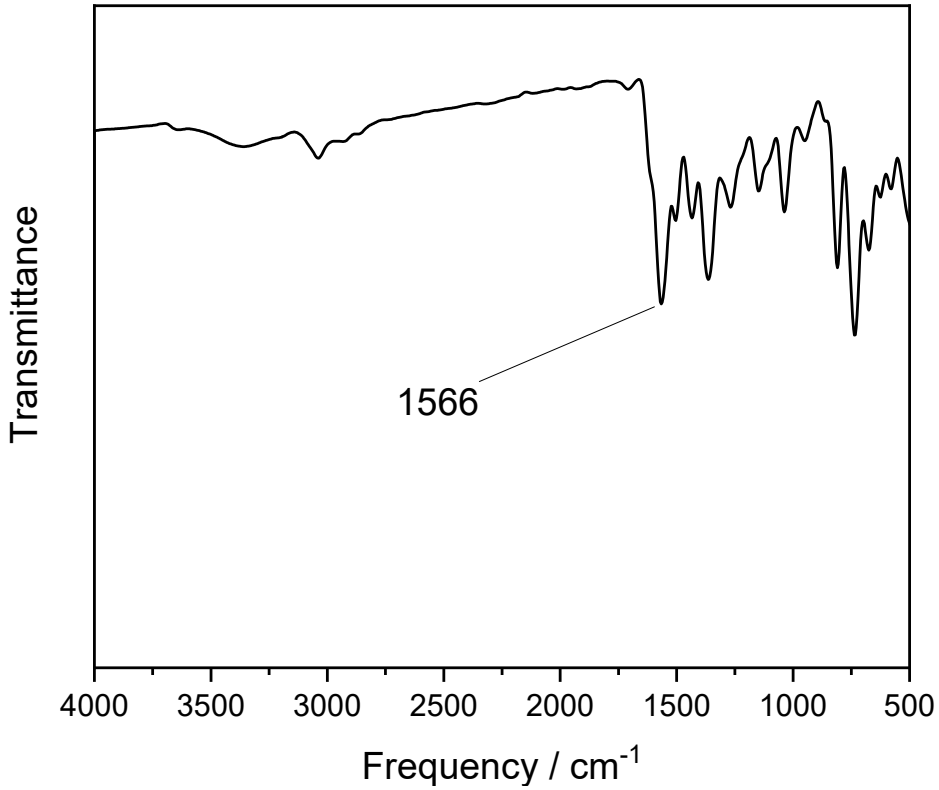

Fig. S25. FTIR spectrum of complex **Ir-piq-L^4**.

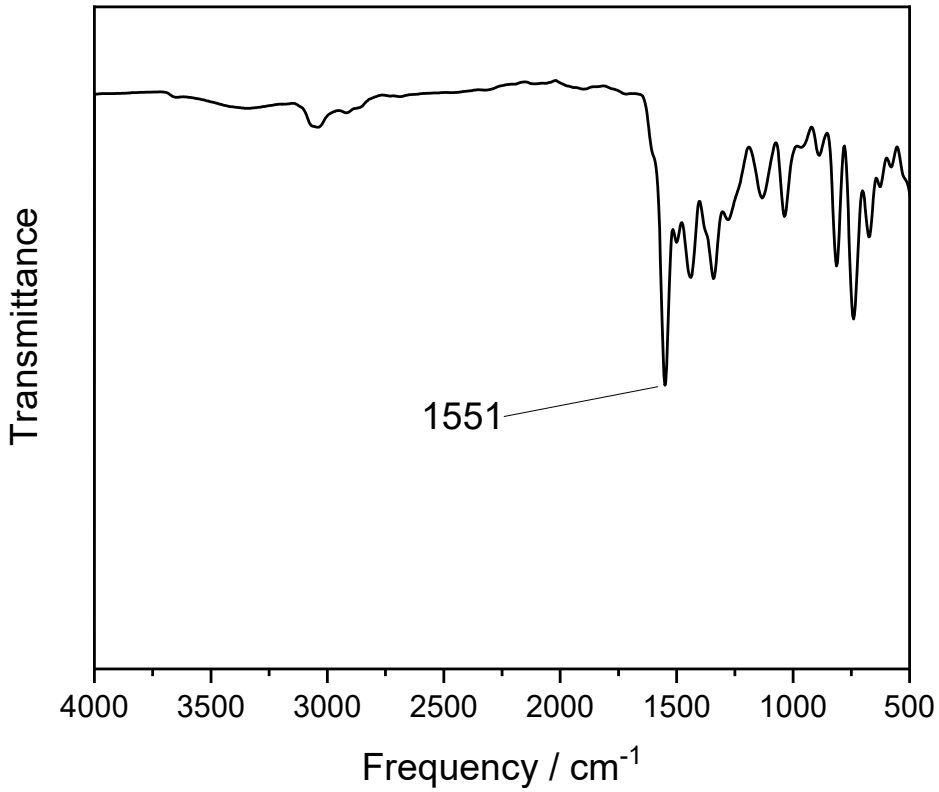

Fig. S26. FTIR spectrum of complex **Ir-piq-L^4-B**.

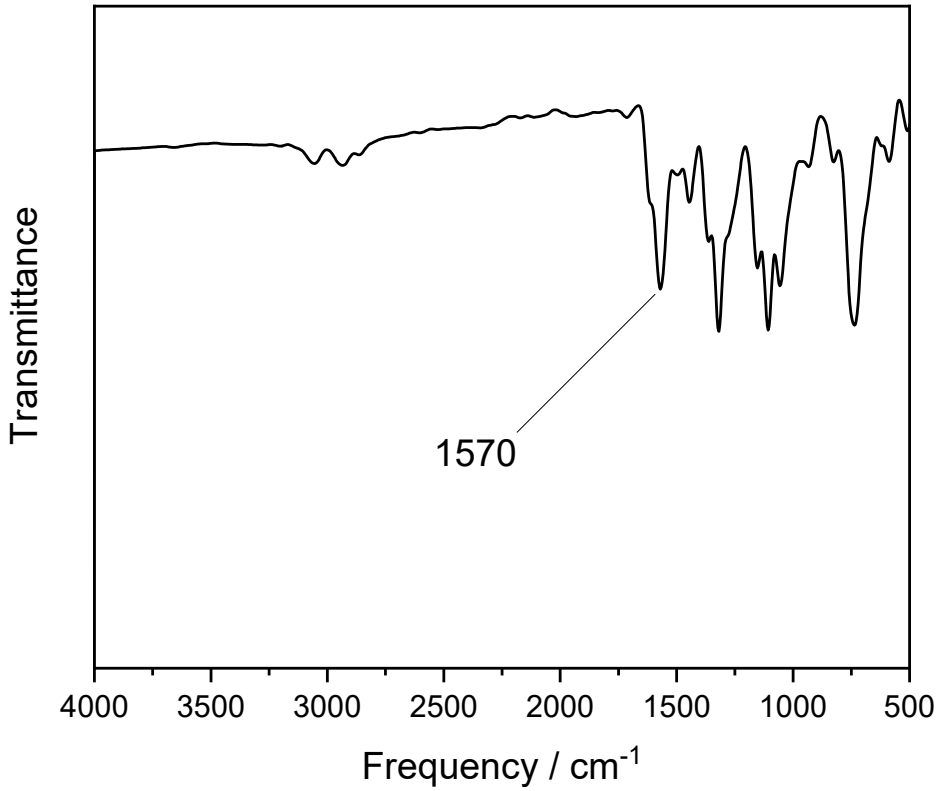

Fig. S27. FTIR spectrum of complex **Ir-ppphen-L^5**.

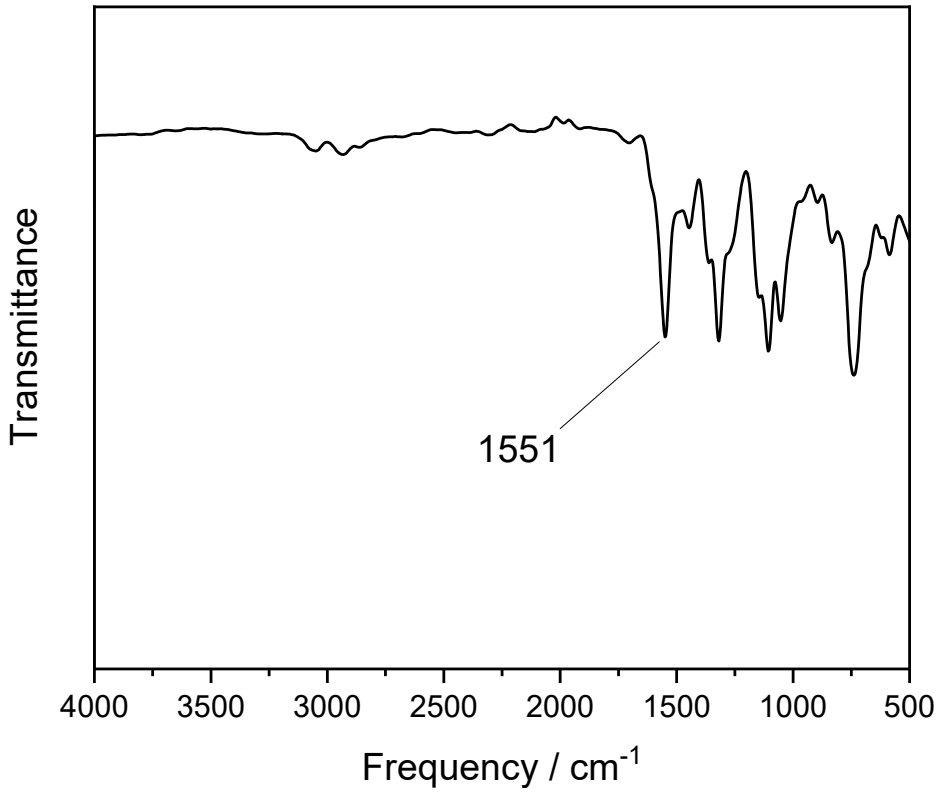

Fig. S28. FTIR spectrum of complex **Ir-pphen-L^5-B**.

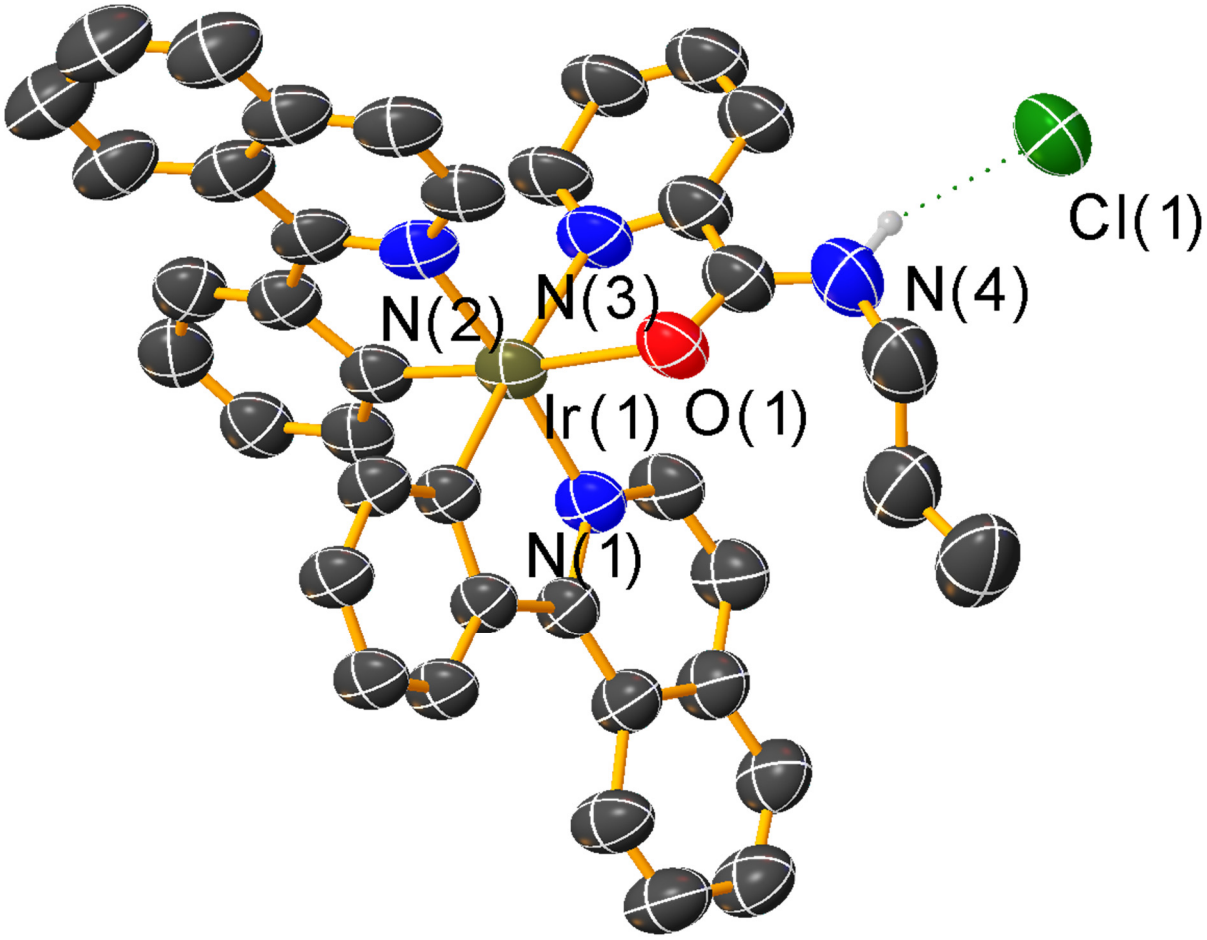

Fig. S29. Molecular structure of **Ir-piq-L^{3}H-B**, determined by single-crystal X-ray diffraction. Thermal ellipsoids are shown at the 50% probability level. Hydrogen atoms bonded to carbon were omitted for clarity.

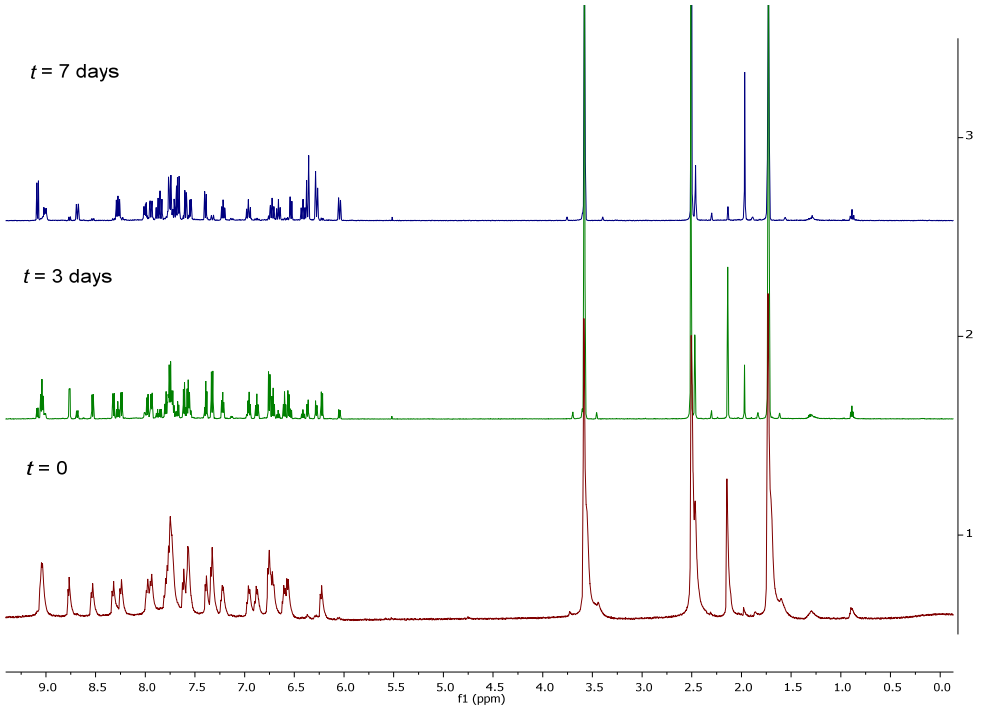

Fig. S30. Evolution of the ^{1}H NMR spectra of **Ir-piq-L^{4}-B** while heating in THF-*d*$_{8}$ at 65 °C for 7 days.

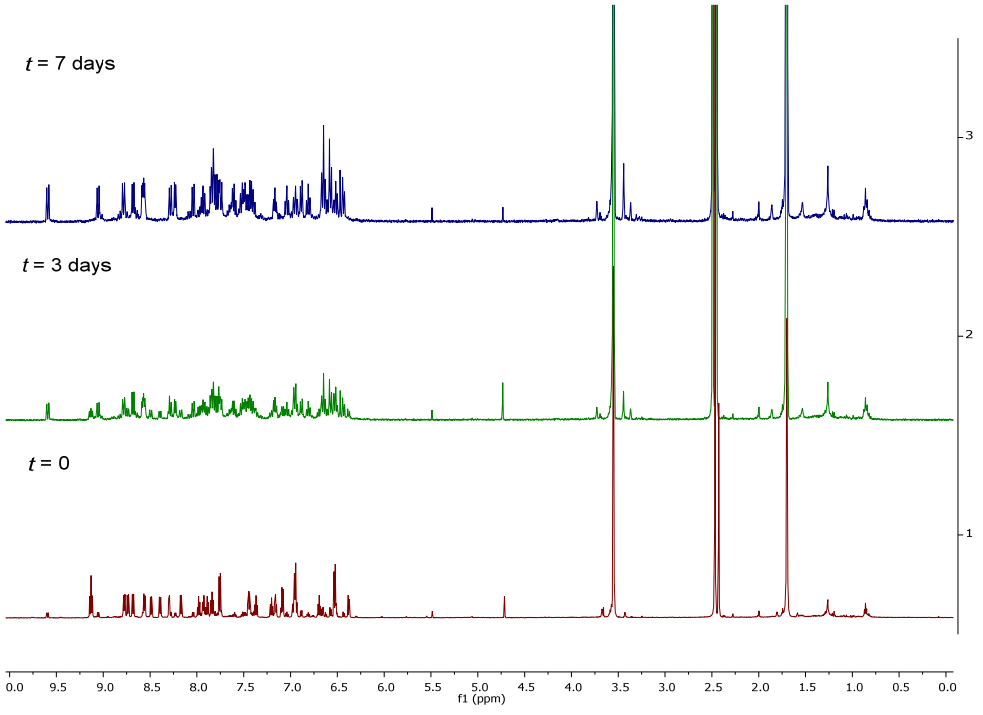

Fig. S31. Evolution of the ^{1}H NMR spectra of **Ir-pphen-L^{5}-B** while heating in THF-*d*$_{8}$ at 65 °C for 7 days.

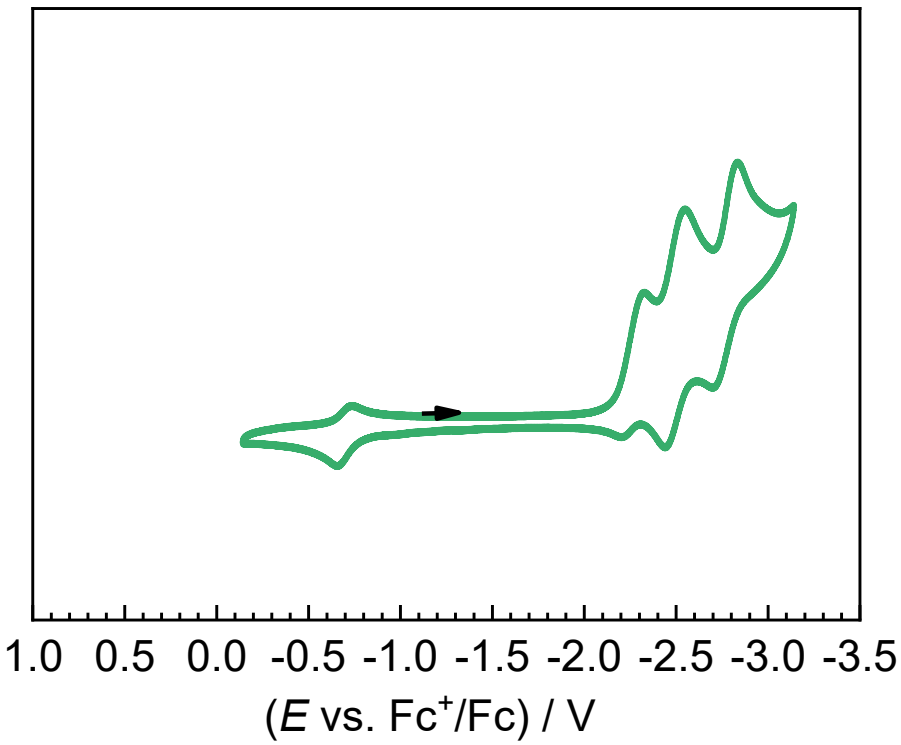

Fig. S32. Cyclic voltammogram of **Ir-piq-L^{6}** in THF with 0.1 M $TBAPF_6$ electrolyte. The arrow indicates the scan direction.

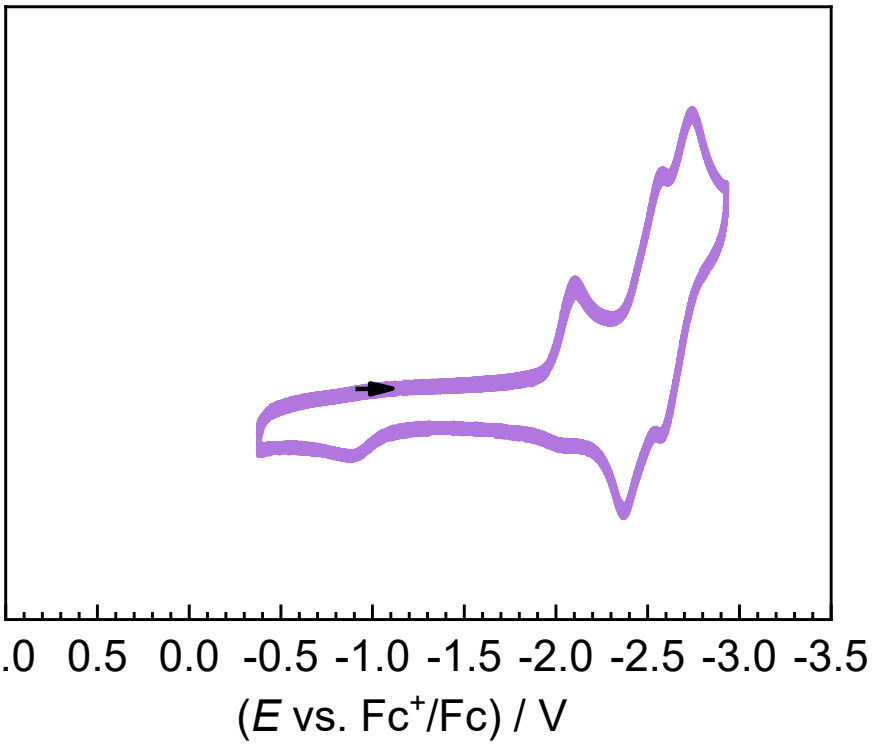

Fig. S33. Cyclic voltammogram of **Ir-piq-L^{3}H-B** in THF with 0.1 M $TBAPF_6$ electrolyte. The arrow indicates the scan direction.

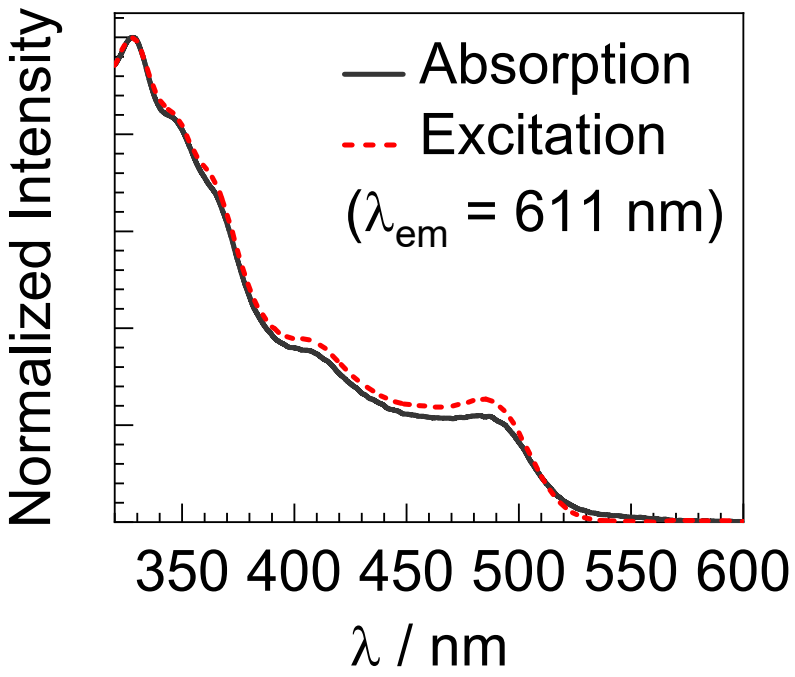

Fig. S34. Overlaid, normalized UV–vis absorption (black solid line) and excitation (red dashed line) spectra of **Ir-btp-L[1]**, recorded in toluene at room temperature.

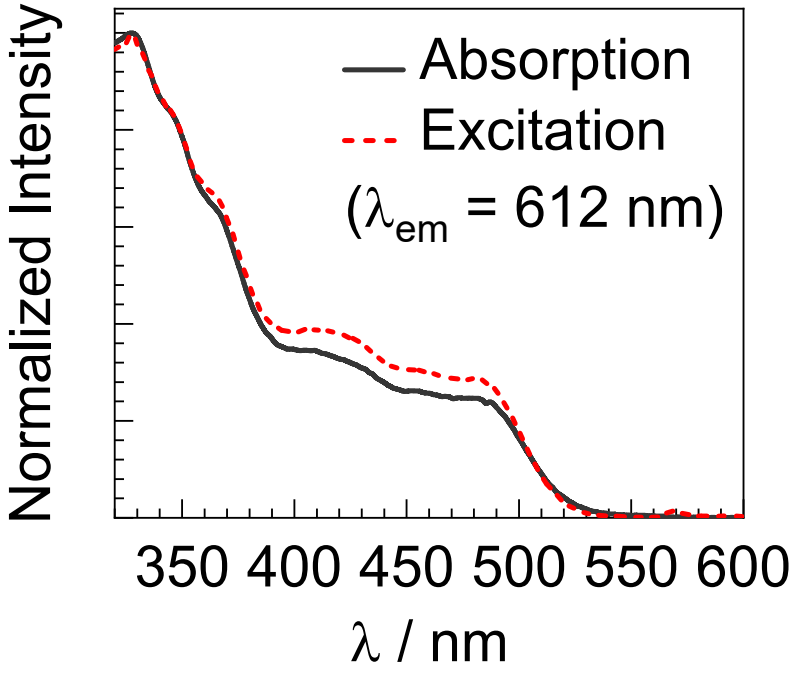

Fig. S35. Overlaid, normalized UV–vis absorption (black solid line) and excitation (red dashed line) spectra of **Ir-btp-L[2]**, recorded in toluene at room temperature.

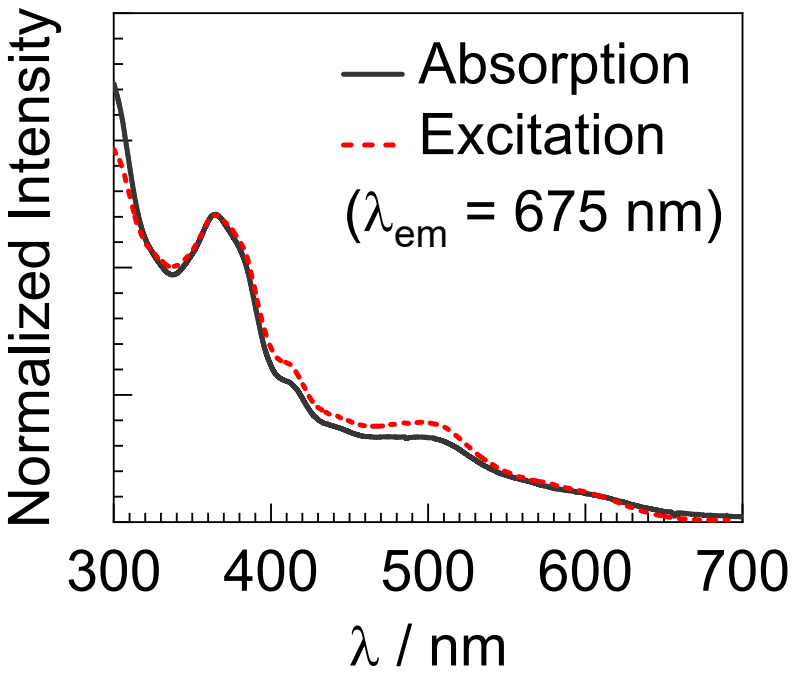

Fig. S36. Overlaid, normalized UV–vis absorption (black solid line) and excitation (red dashed line) spectra of **Ir-pphen-L[1]**, recorded in toluene at room temperature.

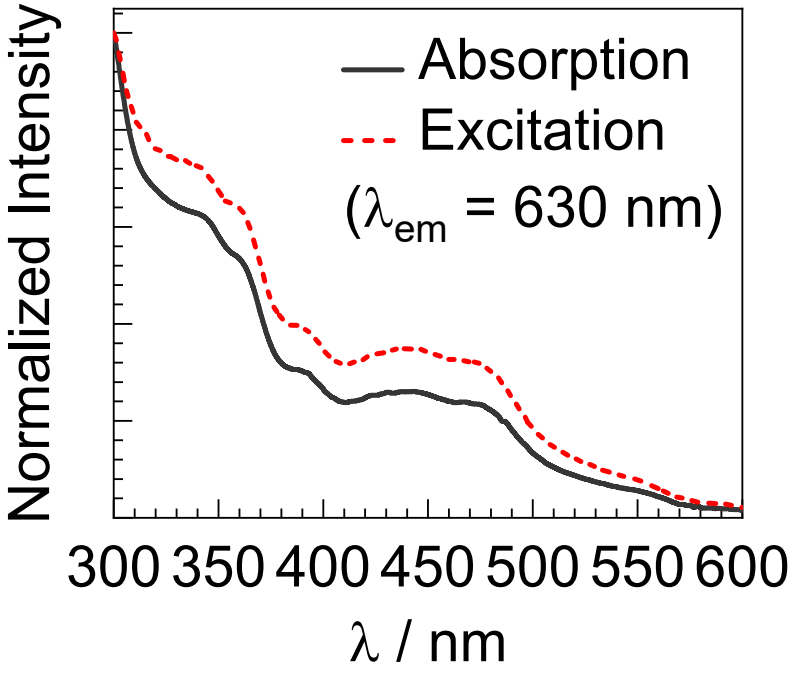

Fig. S37. Overlaid, normalized UV–vis absorption (black solid line) and excitation (red dashed line) spectra of **Ir-piq-L[6]**, recorded in toluene at room temperature.

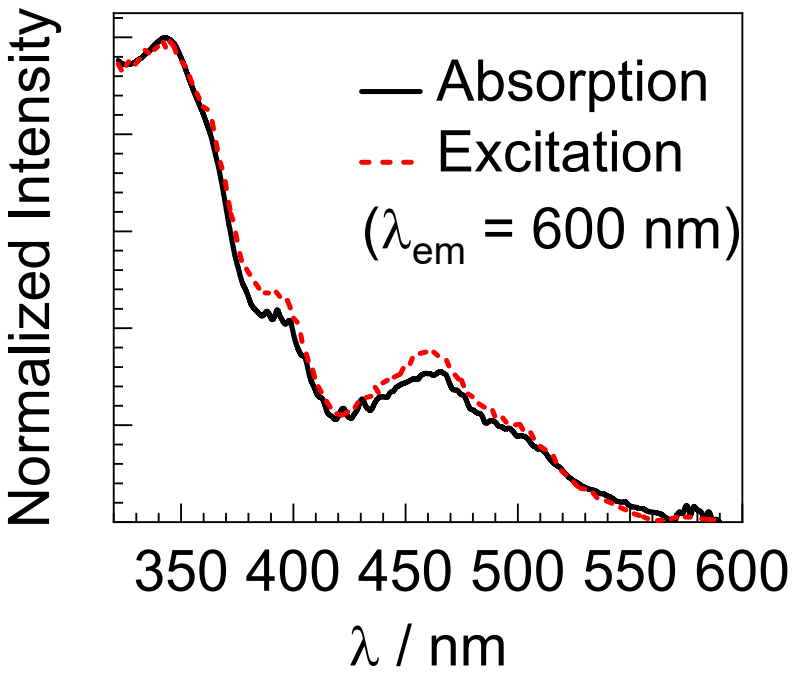

Fig. S38. Overlaid, normalized UV–vis absorption (black solid line) and excitation (red dashed line) spectra of **Ir-piq-L^{3}H-B**, recorded in toluene at room temperature.

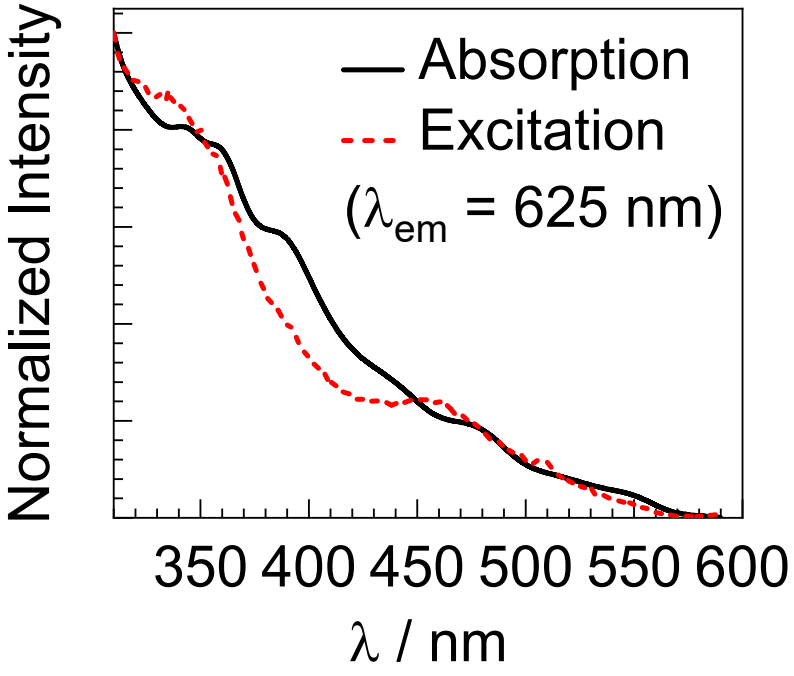

Fig. S39. Overlaid, normalized UV–vis absorption (black solid line) and excitation (red dashed line) spectra of **Ir-piq-L^4-B**, recorded in toluene at room temperature.

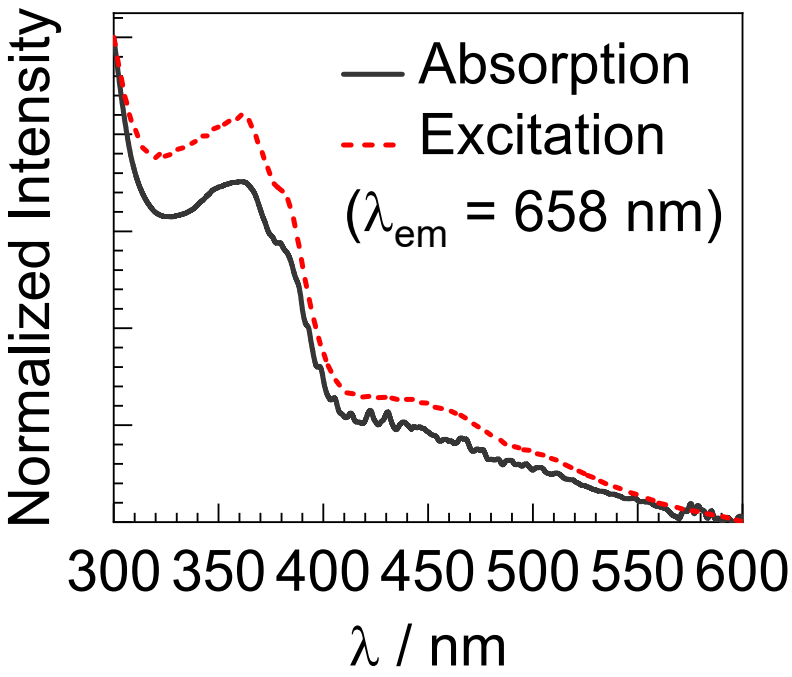

Fig. S40. Overlaid, normalized UV–vis absorption (black solid line) and excitation (red dashed line) spectra of **Ir-pphen-L^5**, recorded in toluene at room temperature.

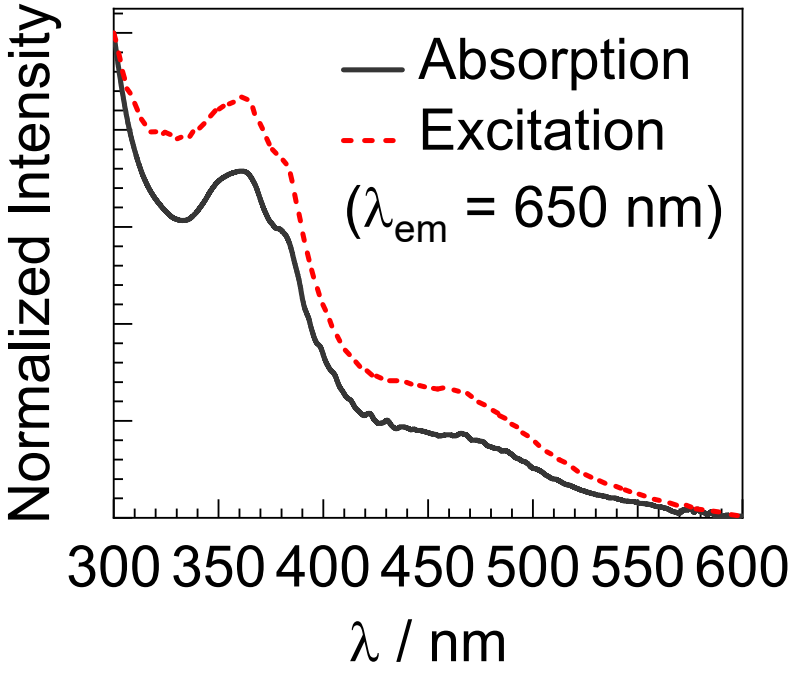

Fig. S41. Overlaid, normalized UV–vis absorption (black solid line) and excitation (red dashed line) spectra of **Ir-pphen-L^5-B**, recorded in toluene at room temperature.

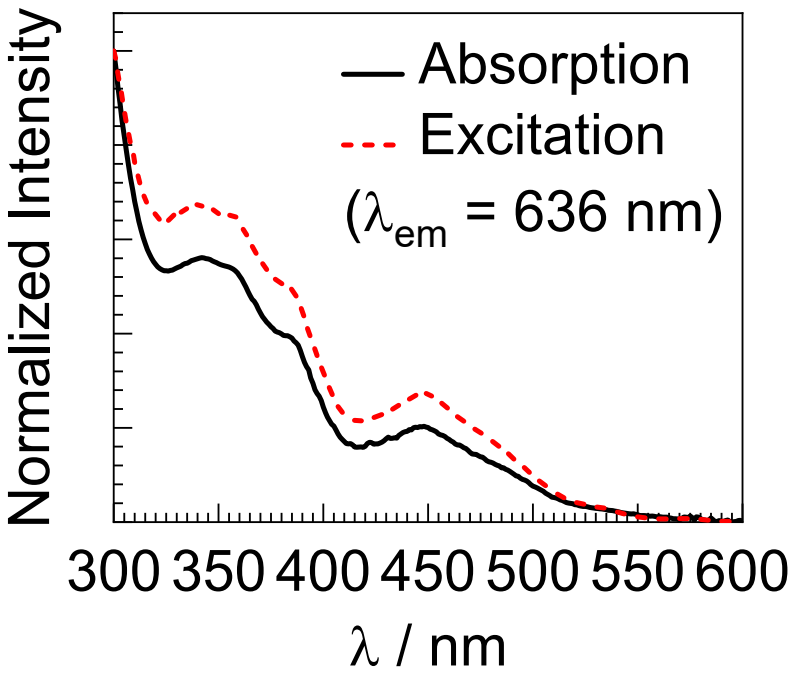

Fig. S42. Overlaid, normalized UV–vis absorption (black solid line) and excitation (red dashed line) spectra of **Ir-piq-L**[7], recorded in toluene at room temperature.

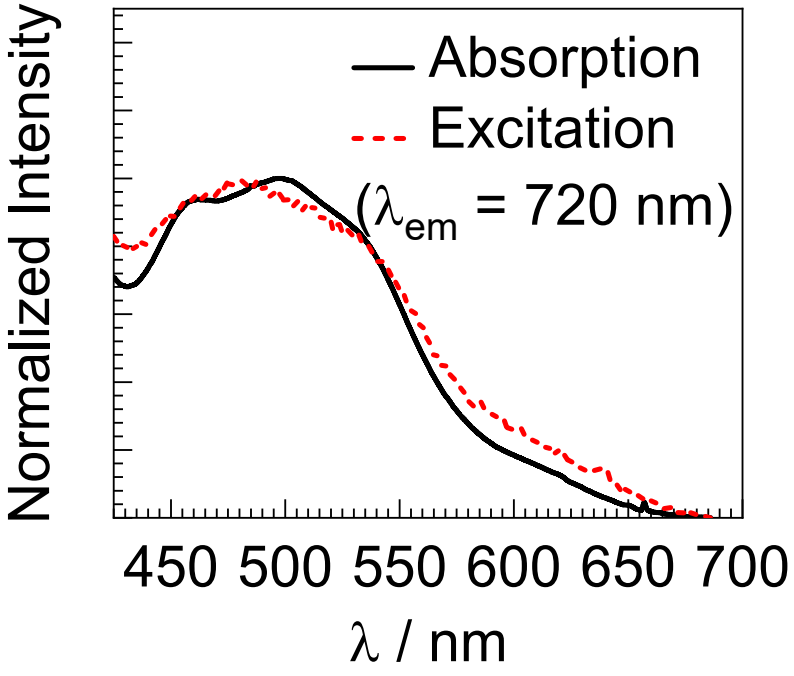

Fig. S43. Overlaid, normalized UV–vis absorption (black solid line) and excitation (red dashed line) spectra of **Ir-piq-L**[8], recorded in toluene at room temperature.

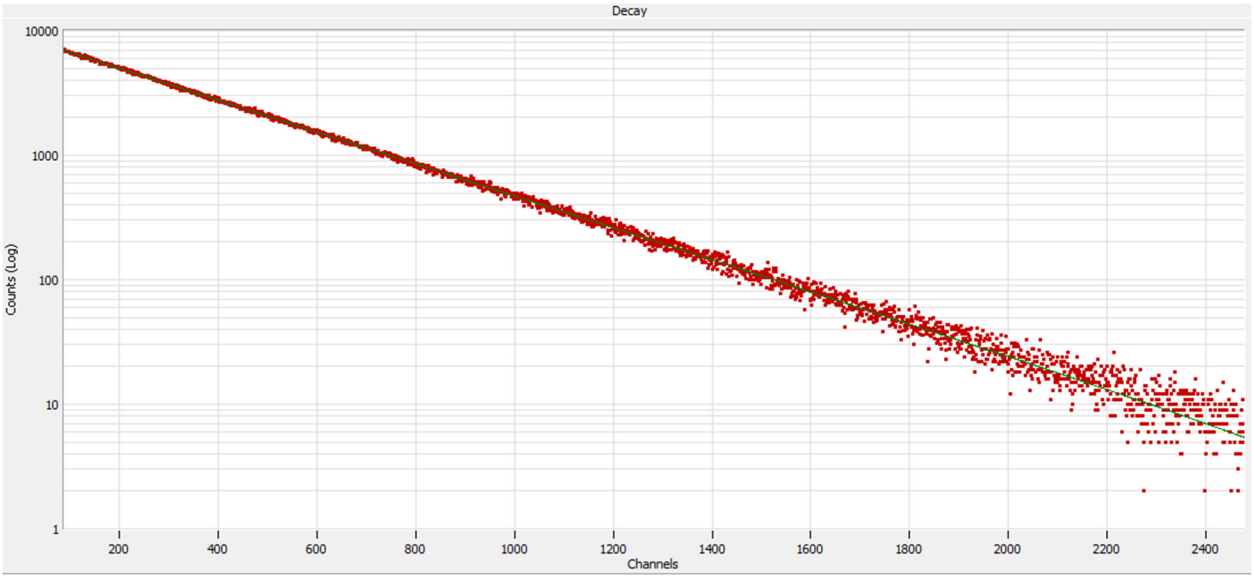

Figure S44. Photoluminescence decay trace for complex **Ir-btp-L[1]**, recorded in toluene solution at room temperature with 390 nm excitation. The raw decay trace is shown in red, with the best-fit line displayed in green.

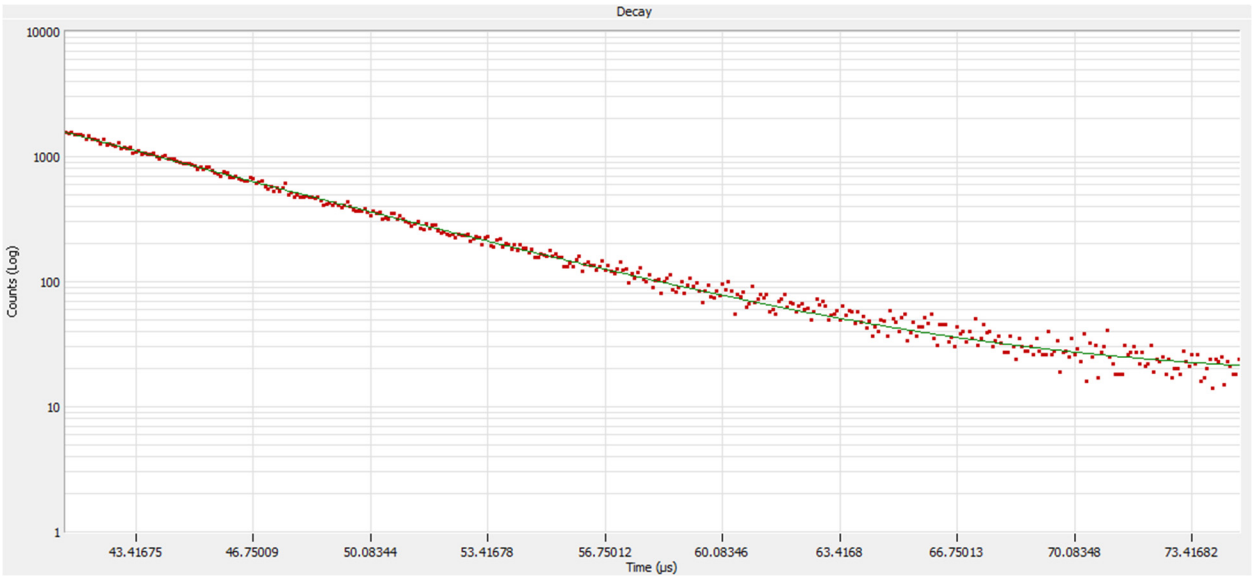

Figure S45. Photoluminescence decay trace for complex **Ir-btp-L[1]**, recorded in PMMA film at room temperature with 390 nm excitation. The raw decay trace is shown in red, with the best-fit line displayed in green.

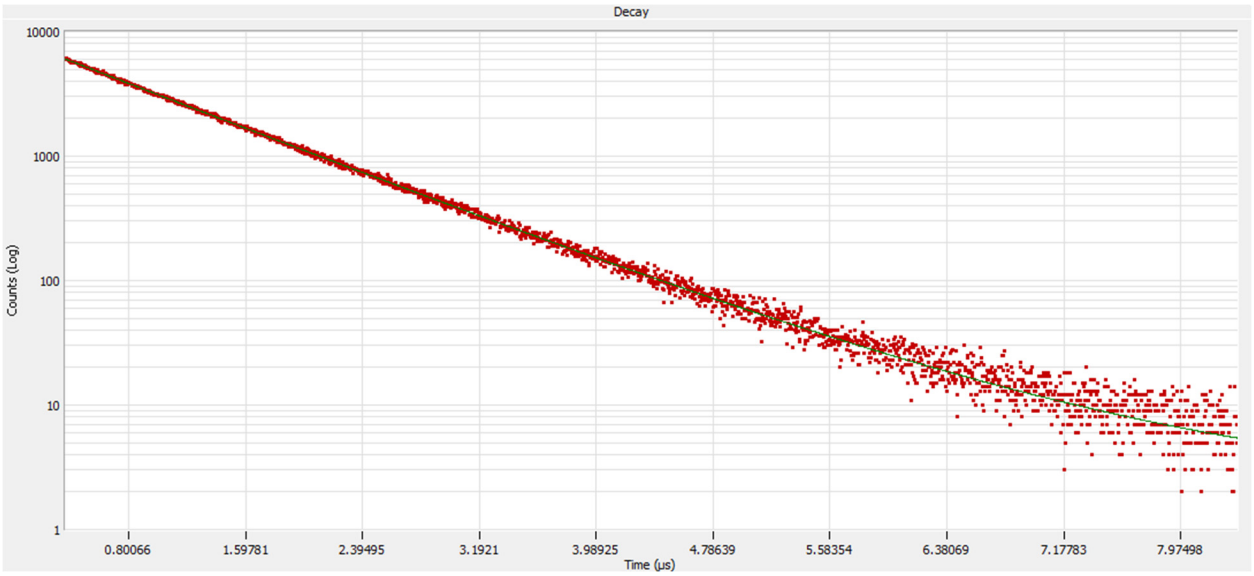

Figure S46. Photoluminescence decay trace for complex **Ir-btp-L^2**, recorded in toluene solution at room temperature with 390 nm excitation. The raw decay trace is shown in red, with the best-fit line displayed in green.

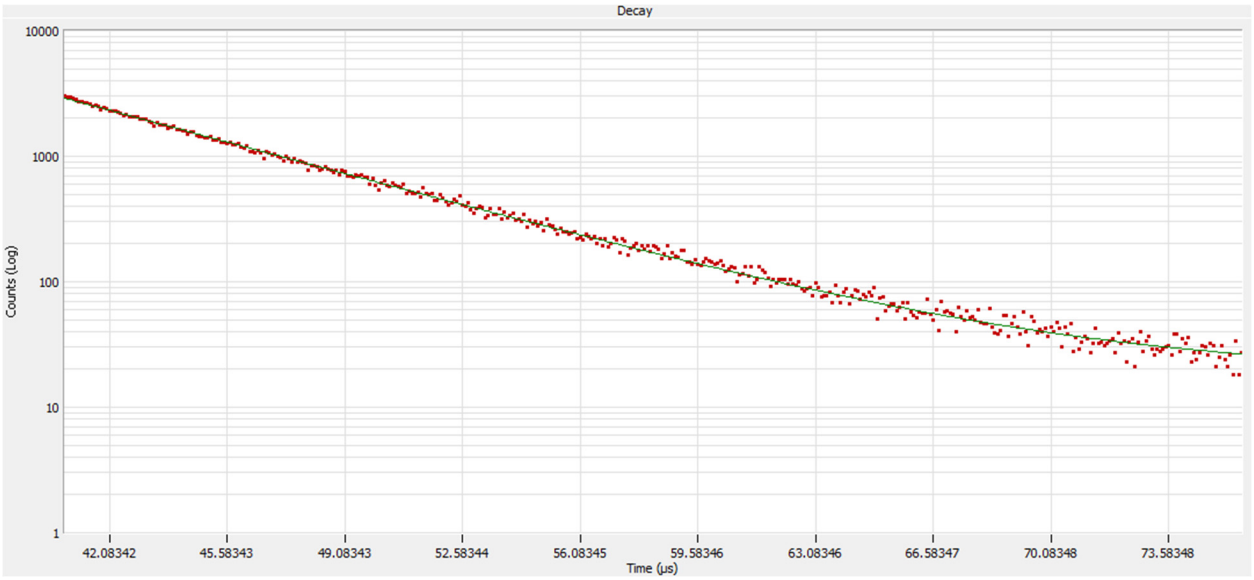

Figure S47. Photoluminescence decay trace for complex **Ir-btp-L^2**, recorded in PMMA film at room temperature with 390 nm excitation. The raw decay trace is shown in red, with the best-fit line displayed in green.

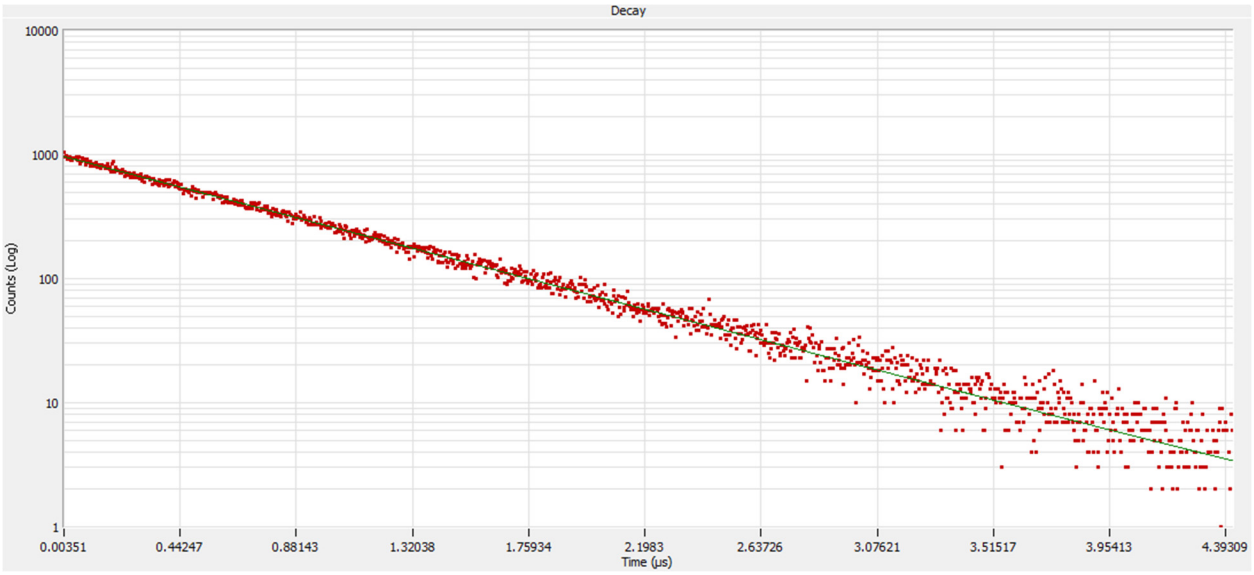

Figure S48. Photoluminescence decay trace for complex **Ir-pphen-L[1]**, recorded in toluene solution at room temperature with 390 nm excitation. The raw decay trace is shown in red, with the best-fit line displayed in green.

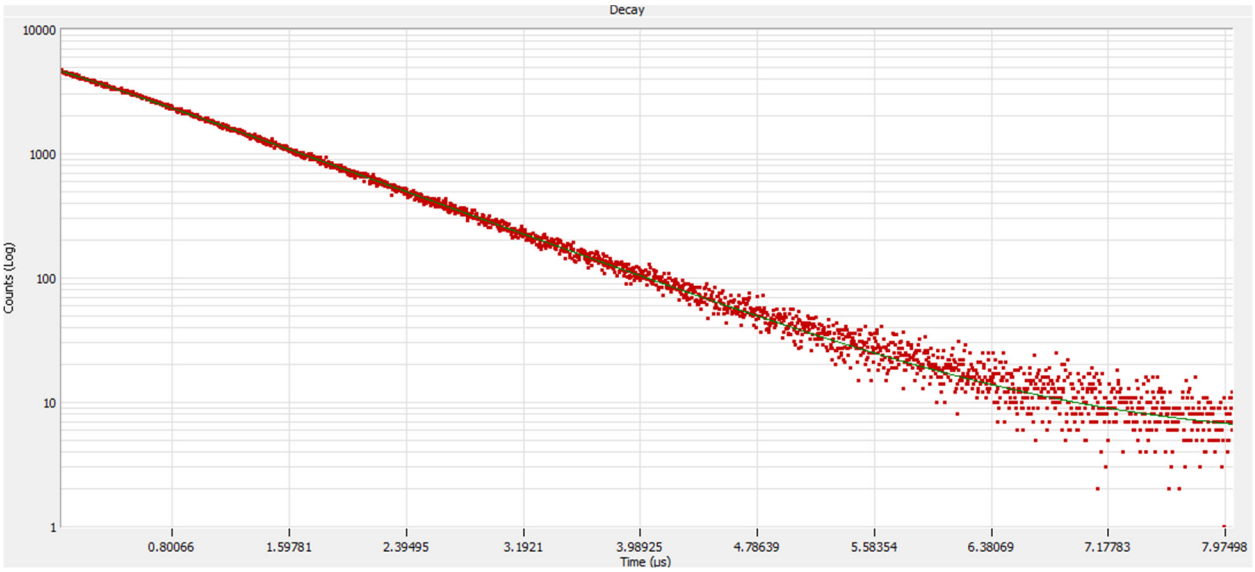

Figure S49. Photoluminescence decay trace for complex **Ir-pphen-L[1]**, recorded in PMMA film at room temperature with 390 nm excitation. The raw decay trace is shown in red, with the best-fit line displayed in green.

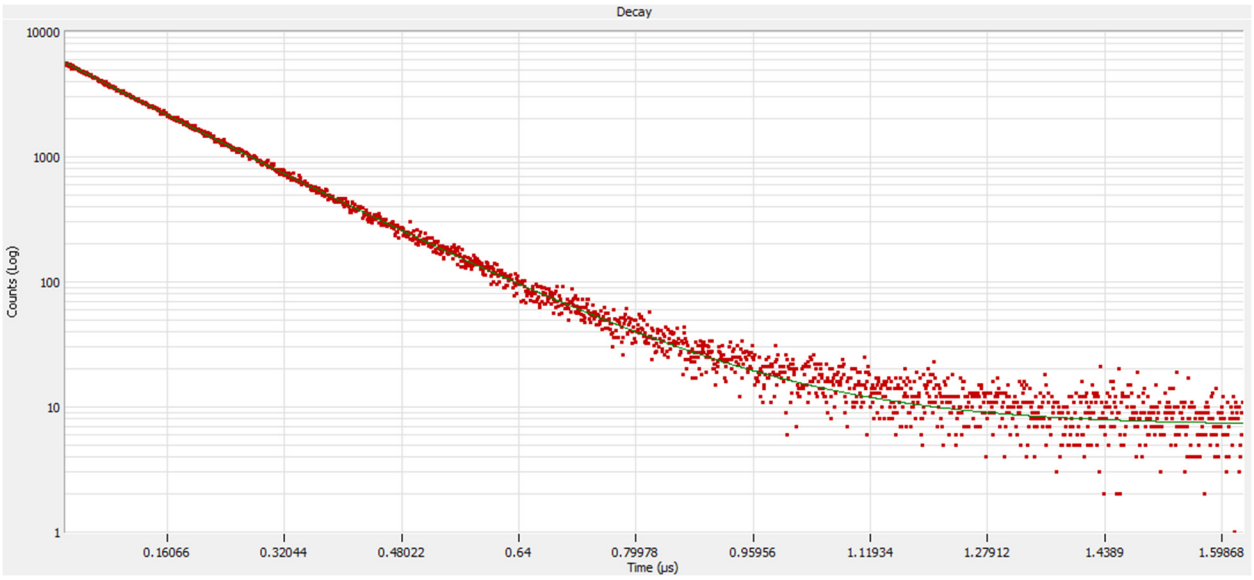

Figure S50. Photoluminescence decay trace for complex **Ir-piq-L[6]**, recorded in toluene solution at room temperature with 390 nm excitation. The raw decay trace is shown in red, with the best-fit line displayed in green.

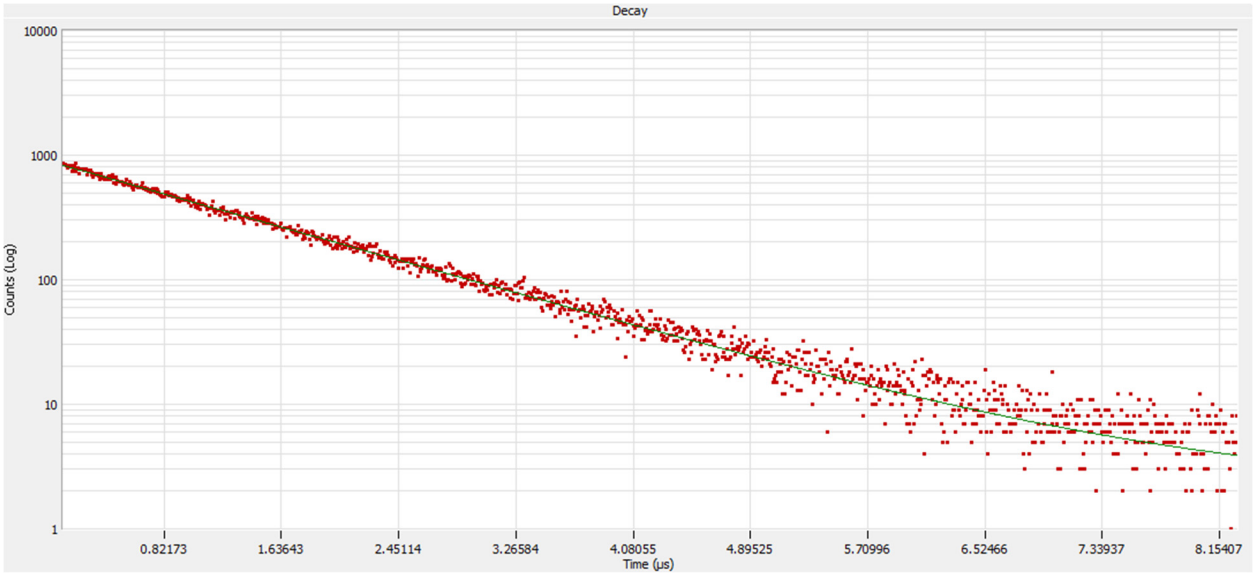

Figure S51. Photoluminescence decay trace for complex **Ir-piq-L[6]**, recorded in PMMA film at room temperature with 390 nm excitation. The raw decay trace is shown in red, with the best-fit line displayed in green.

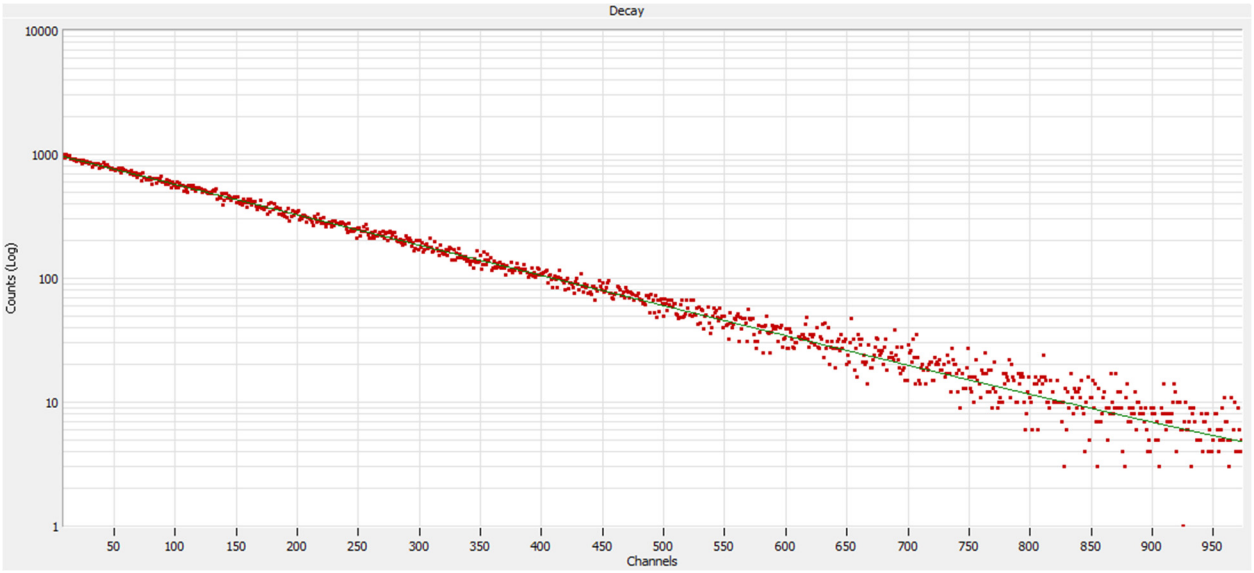

Figure S52. Photoluminescence decay trace for complex **Ir-piq-L^{3}H-B**, recorded in toluene solution at room temperature with 390 nm excitation. The raw decay trace is shown in red, with the best-fit line displayed in green.

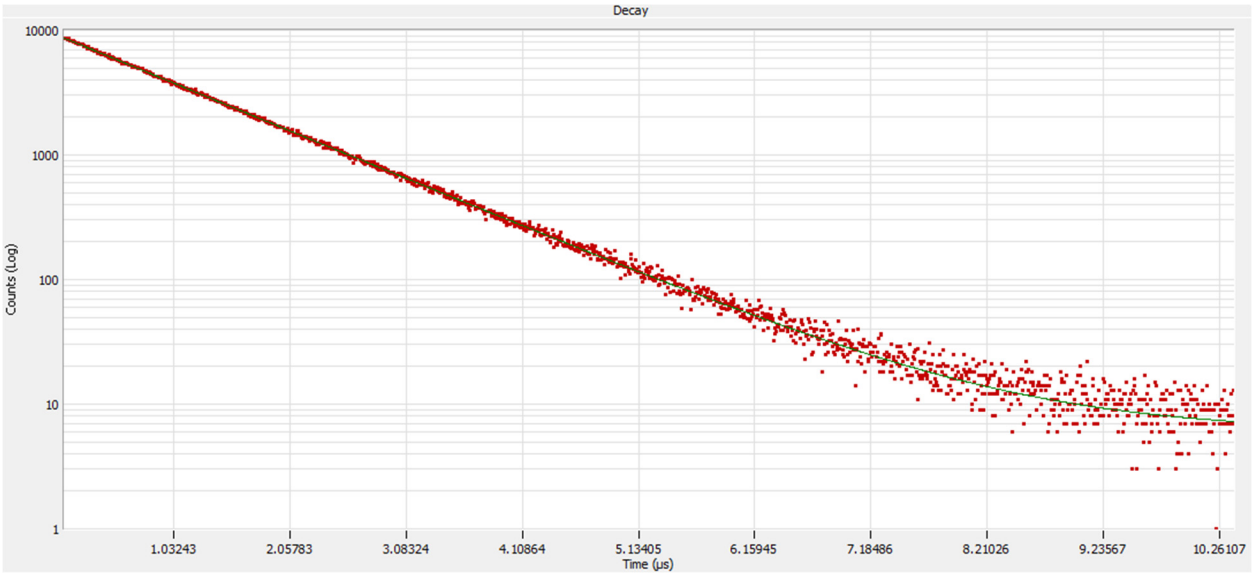

Figure S53. Photoluminescence decay trace for complex **Ir-piq-L^{3}H-B**, recorded in PMMA film at room temperature with 390 nm excitation. The raw decay trace is shown in red, with the best-fit line displayed in green.

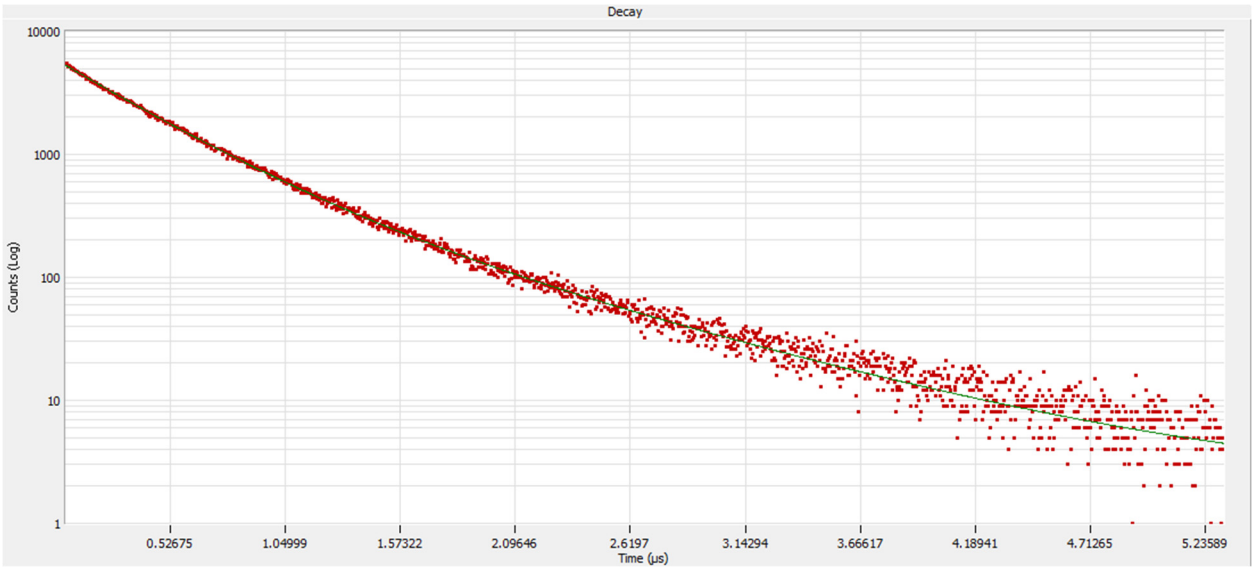

Figure S54. Photoluminescence decay trace for complex **Ir-piq-L^4-B**, recorded in toluene solution at room temperature with 390 nm excitation. The raw decay trace is shown in red, with the best-fit line displayed in green.

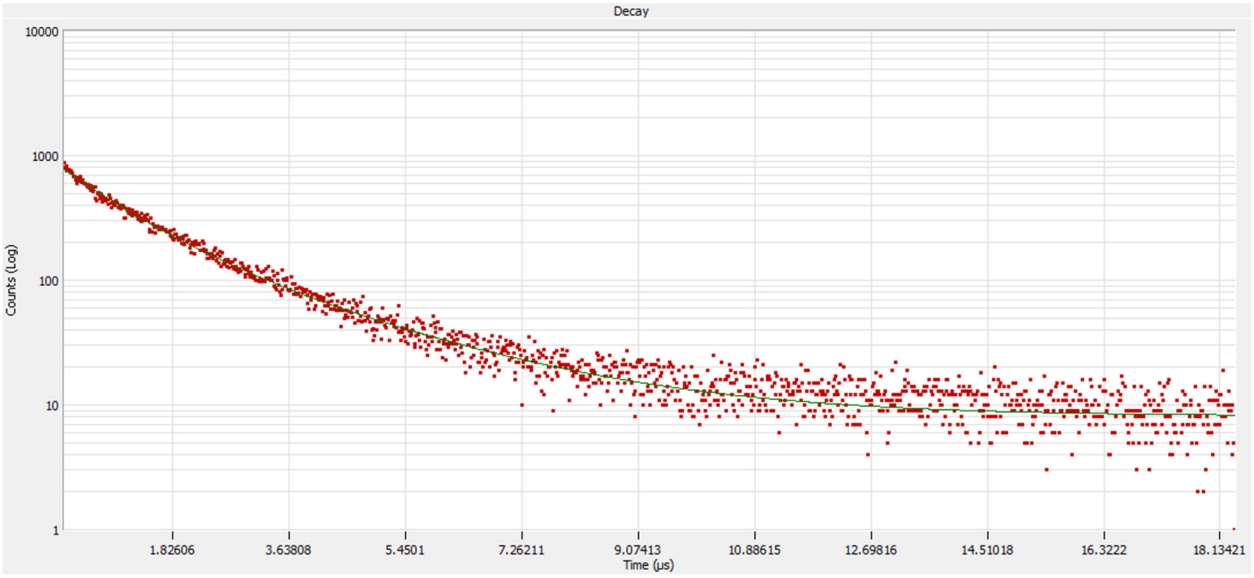

Figure S55. Photoluminescence decay trace for complex **Ir-piq-L^4-B**, recorded in PMMA film at room temperature with 390 nm excitation. The raw decay trace is shown in red, with the best-fit line displayed in green.

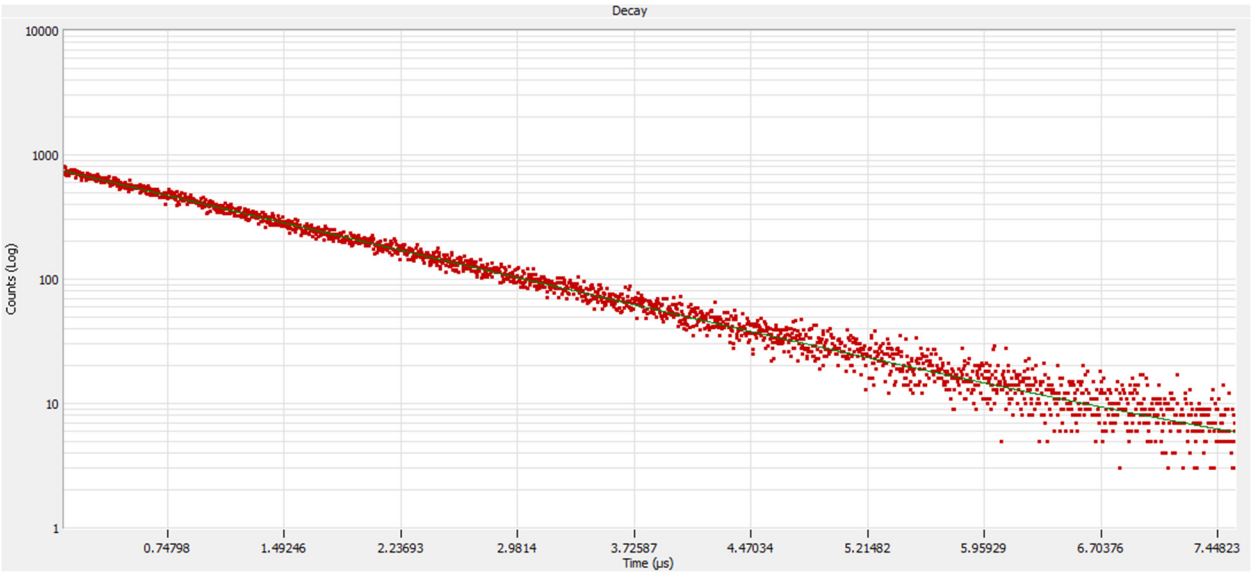

Figure S56. Photoluminescence decay trace for complex **Ir-pphen-L[5]**, recorded in toluene solution at room temperature with 390 nm excitation. The raw decay trace is shown in red, with the best-fit line displayed in green.

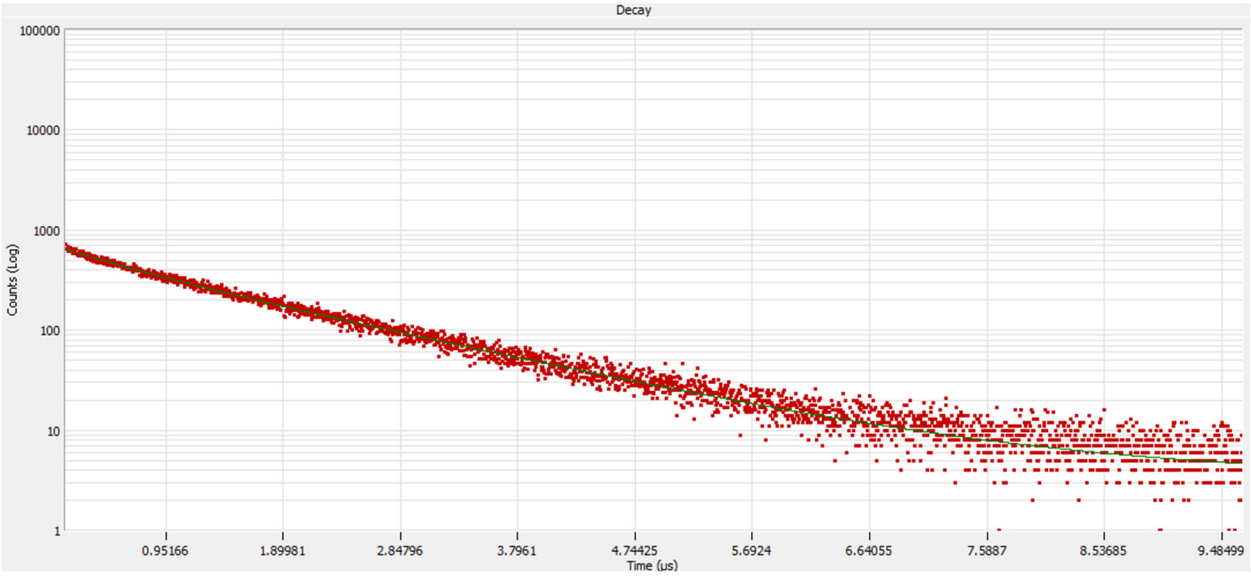

Figure S57. Photoluminescence decay trace for complex **Ir-pphen-L[5]**, recorded in PMMA film at room temperature with 390 nm excitation. The raw decay trace is shown in red, with the best-fit line displayed in green.

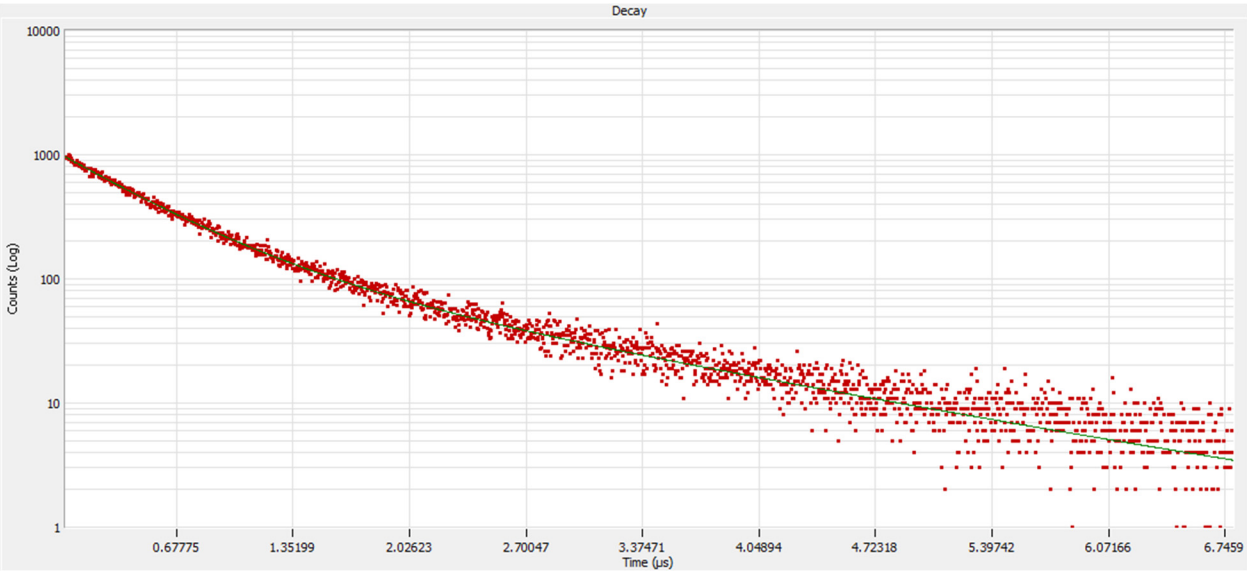

Figure S58. Photoluminescence decay trace for complex **Ir-pphen-L^5-B**, recorded in toluene solution at room temperature with 390 nm excitation. The raw decay trace is shown in red, with the best-fit line displayed in green.

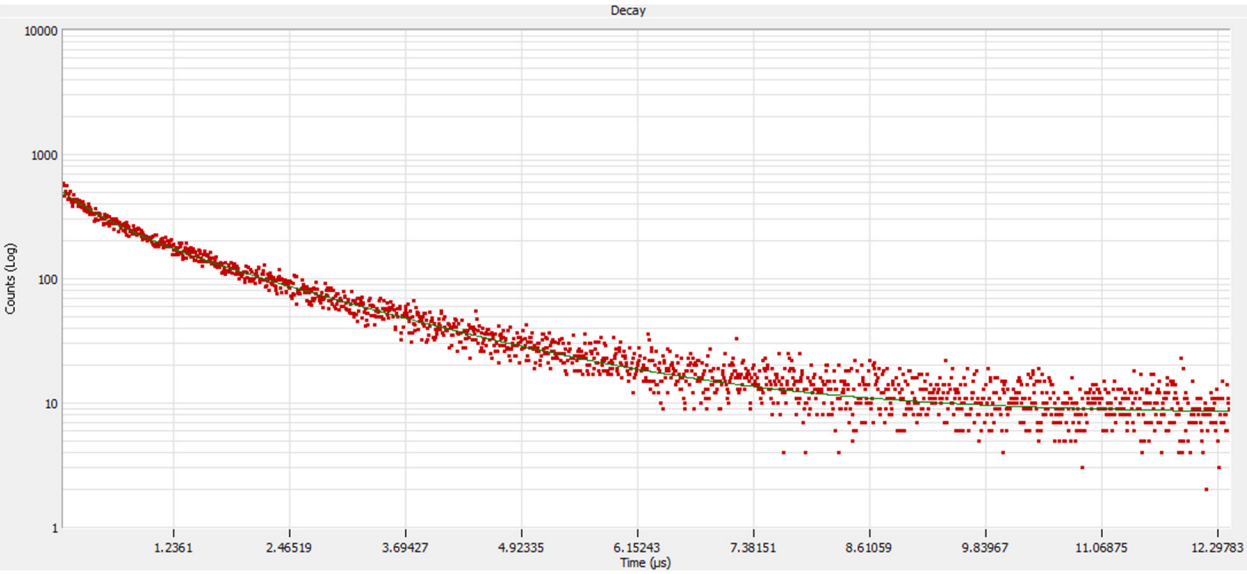

Figure S59. Photoluminescence decay trace for complex **Ir-pphen-L^5-B**, recorded in PMMA film at room temperature with 390 nm excitation. The raw decay trace is shown in red, with the best-fit line displayed in green.

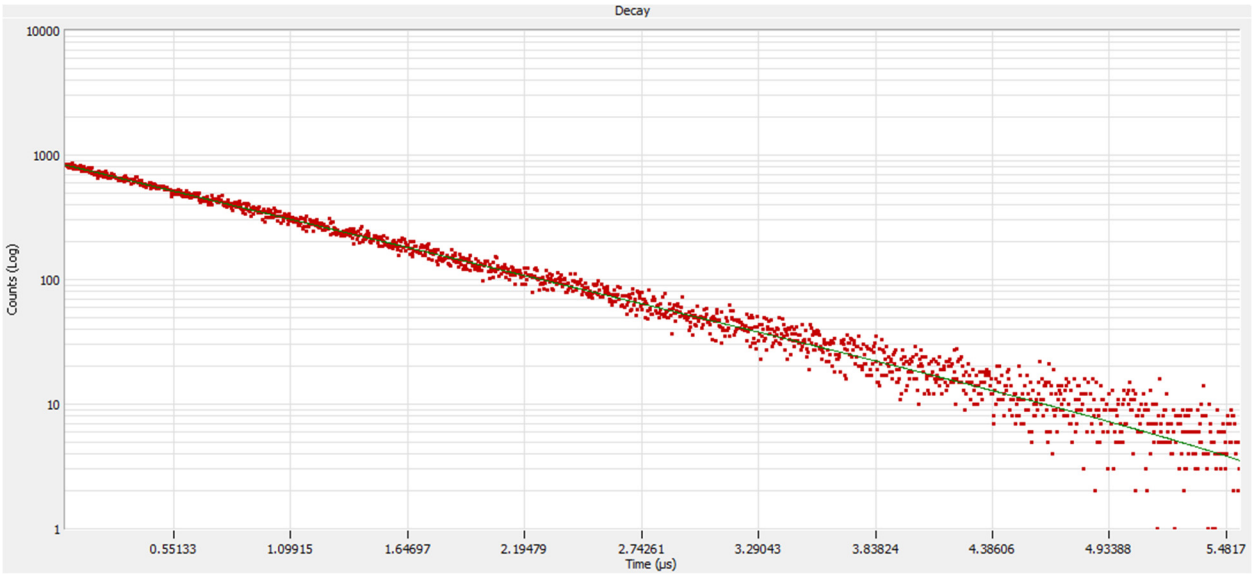

Figure S60. Photoluminescence decay trace for complex **Ir-piq-L**[7], recorded in toluene solution at room temperature with 390 nm excitation. The raw decay trace is shown in red, with the best-fit line displayed in green.

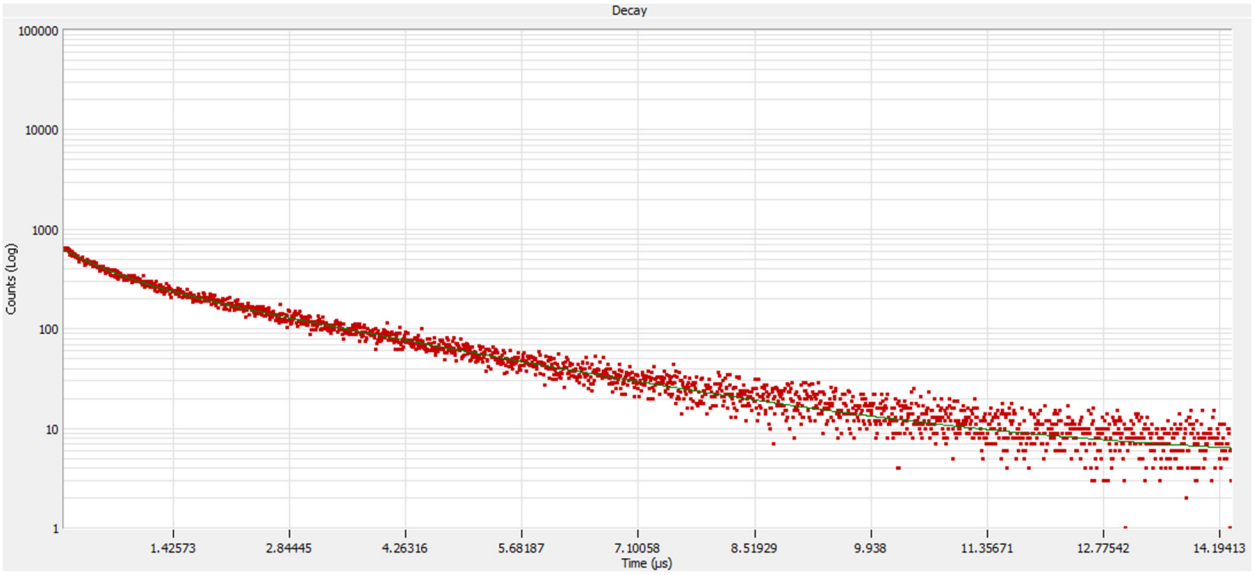

Figure S61. Photoluminescence decay trace for complex **Ir-piq-L**[7], recorded in PMMA film at room temperature with 390 nm excitation. The raw decay trace is shown in red, with the best-fit line displayed in green.

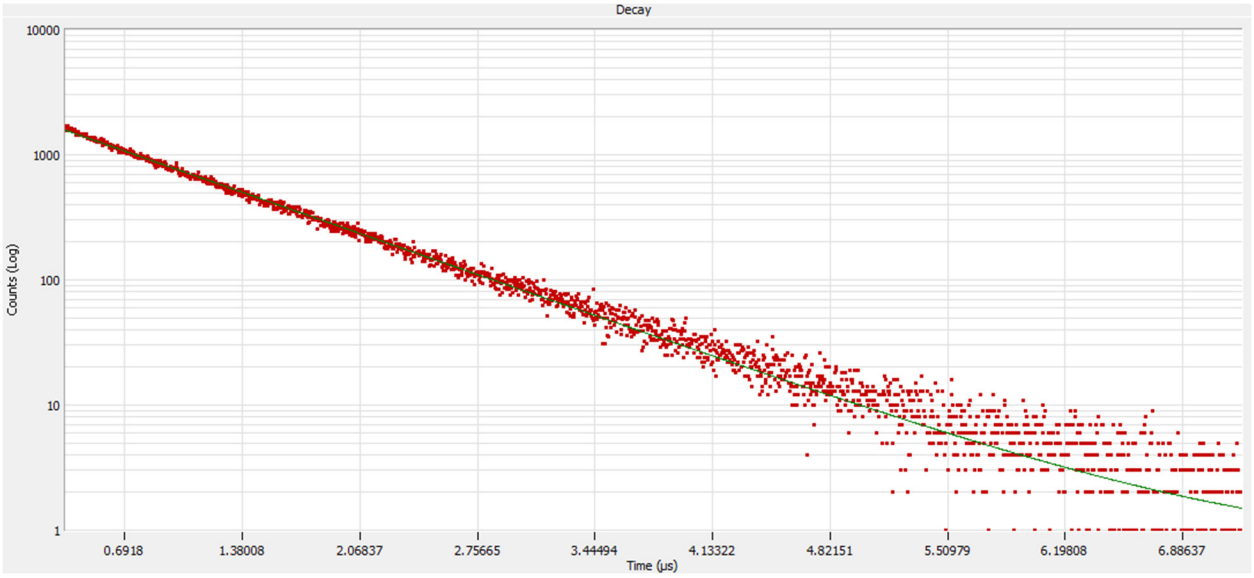

Figure S62. Photoluminescence decay trace for complex **Ir-piq-L[8]**, recorded in toluene solution at room temperature with 390 nm excitation. The raw decay trace is shown in red, with the best-fit line displayed in green.

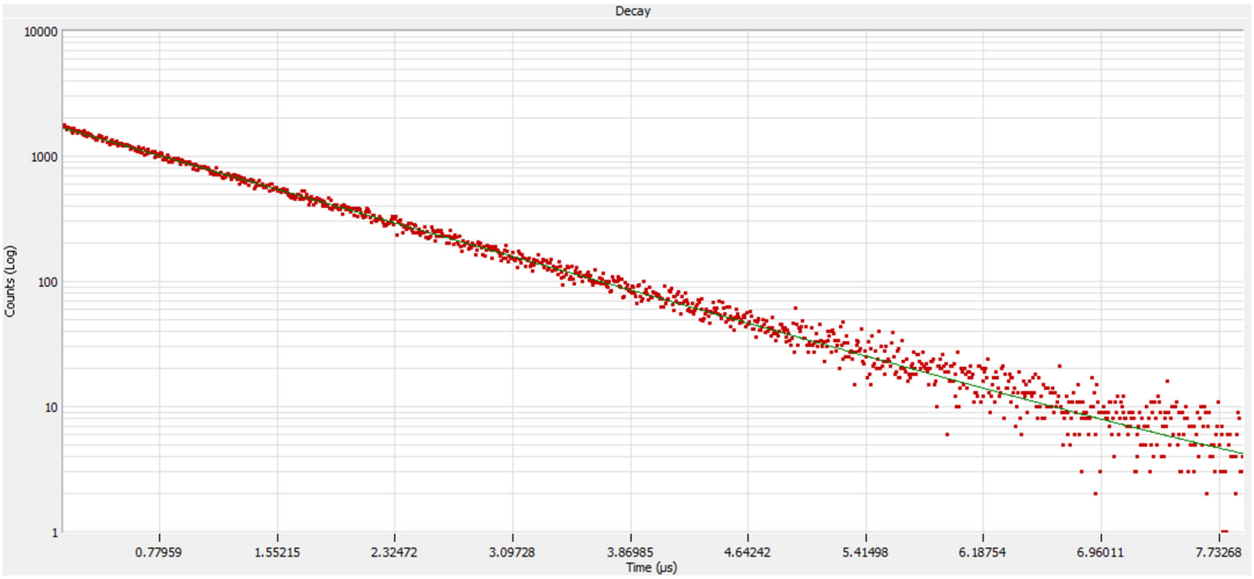

Figure S63. Photoluminescence decay trace for complex **Ir-piq-L[8]**, recorded in PMMA film at room temperature with 390 nm excitation. The raw decay trace is shown in red, with the best-fit line displayed in green.

ESI References

1 M. Nonoyama, Benzo[h]quinolin-10-yl-N Iridium(III) Complexes, *BCSJ*, 1974, **47**, 767–768.

2 C. Jiang, S. Yoon, Y. H. Nguyen and T. S. Teets, Modular Imine Chelates with Variable Anionic Donors Promote Red Phosphorescence in Cyclometalated Iridium Complexes, *Inorg. Chem.*, 2023, **62**, 11278–11286.

3 X. Meng, Y.-J. Lin and G.-X. Jin, Syntheses and molecular structures of 18/16-electron half-sandwich iridium(III) complexes with chelating anilido-imine ligands, *Journal of Organometallic Chemistry*, 2008, **693**, 2597–2602.

4 B. C. E. Makhubela, A. M. Jardine, G. Westman and G. S. Smith, Hydroformylation of 1-octene using low-generation Rh(I) metallodendritic catalysts based on a tris-2-(2-pyridyliminoethyl)amine scaffold, *Dalton Trans.*, 2012, **41**, 10715–10723.

5 P. Altmann, M. Cokoja and F. E. Kühn, Halide substituted Schiff-bases: Different activities in methyltrioxorhenium(VII) catalyzed epoxidation via different substitution patterns, *Journal of Organometallic Chemistry*, 2012, **701**, 51–55.

6 P. G. Seybold and M. Gouterman, Porphyrins: XIII: Fluorescence spectra and quantum yields, *Journal of Molecular Spectroscopy*, 1969, **31**, 1–13.

7 G. M. Sheldrick, Crystal structure refinement with SHELXL, *Acta Cryst C*, 2015, **71**, 3–8.

8 A. L. Spek, Structure validation in chemical crystallography, *Acta Cryst D*, 2009, **65**, 148–155.